

# Chapter 1

## Introduction

The wireless communication industry has been rapidly growing during the past years. Cellular phones, pagers, cordless phones and satellite communications focusing on voice service for customers are very popular. So we can say that the wireless communications have become a part of our daily lives [1]. Obviously, the wireless communication services possess the ability to support user mobility while a wired system lacks of this flexibility. Currently, due to the increasing demands of digital multimedia communication and Internet, data services become important. In the future, wireless local area network (WLAN), digital broadcasting, satellite, cellular and other access systems will be connected together to provide integrated and seamless services via a ubiquitous network environment, in which we can utilize convenient services anytime and anywhere through various types of network connections [2]–[4]. Therefore, a reliable link between transmitter and receiver with high speed data rate, and a large capacity allowing more users to use the services simultaneously are necessary conditions to ensure the success of these services.

Multiple access techniques allow many users to communicate with each other simultaneously through shared and limited resources without serious interferences among users. There are three major multiple access techniques [5]–[8] as follows:

### **1. Time division multiple access (TDMA)**

This multiple access technique divides the channel resource into time slots, and in each slot only one user is allowed to transmit or receive.

### **2. Frequency division multiple access (FDMA)**

This multiple access technique divides the channel resource into frequency band (or channel), and different frequency bands are allocated to different users on a continuous-time basis.

### **3. Code division multiple access (CDMA)**

This multiple access technique assigns a unique pseudorandom code to each intended user, and all users use the same carrier frequency and may transmit simultaneously. At the receiver, the desired signal is extracted by correlating the transmitted signal with a local replica of the desired user's code.

A signal propagating through the wireless channel will be subject to additive background noise, and may experience signal fading, multipath spread, cochannel interference, etc. The effect of combined channel impairments becomes more severe when the transmitter/receiver is in motion and data rate is high, which leads to significant degradation in system performance. As remedies, signal processing techniques are usually used to improve the link performance in hostile mobile radio environments. Diversity and equalization are two main techniques [8], [9] that can be used individually or together to improve received signal quality.

## **1.1 Overview of Diversity Techniques**

In a multipath fading channel, the signal transmission errors occur in reception when the channel is in a deep fade. Diversity techniques can be employed to reduce the depth and duration of the fades experienced by a receiver. That is, if the receiver can have several replicas of the same information-bearing signal transmitted through independently fading channels by using diversity techniques, the probability that all the independently faded signal components experience deep fading simultaneously will be greatly reduced. Four basic diversity techniques [8]–[11] of interest are described as below:

### **1. Space diversity.**

The information-bearing signal is transmitted by using multiple transmitting or receiving antennas (or both). The space separation between adjacent antennas should be large enough to assure the independence of possible fading events

occurring in the channel, and usually a separation of a few wavelengths is needed between adjacent antennas. This space diversity technique does not require extra channel capacity; however, extra antennas or receiver equipments are needed.

## **2. Frequency diversity.**

The information-bearing signal is transmitted simultaneously over more than one carrier frequency. The separation between adjacent carrier frequencies should be larger than the coherence bandwidth of the channel to provide independently fading versions of the signal. By using redundant signal transmission, this diversity technique improves link quality at the expense of extra frequency bandwidth.

## **3. Time diversity.**

The information-bearing signal is transmitted repeatedly at time spacing that exceeds the coherence time of the channel, so that multiple repetitions of the signal will be received with independent fading conditions. This diversity technique may be linked to the use of a repetition code for forward error-control correction coding. By using redundant signal transmission, this diversity technique improves link quality at the cost of extra channel capacity (in terms of transmission time).

## **4. Path diversity.**

In CDMA spread spectrum systems, the spreading codes are designed to have a low cross correlation among chips. The spread spectrum signal can resolve multipath components that are separated in time by more than one chip duration. A RAKE receiver can extract the received signal components from different propagation paths by using code correlation and then combine the signal components constructively. In practice, this technique exploits path diversity to reduce the transmission power and increase the system capacity in CDMA systems.

Through the use of diversity techniques, several replicas of the independent faded signals are obtained at the output of the demodulators. The next step is to

combine these statistically independent signal components in order to improve the symbol detection capability in the receiver. Three linear combining techniques [11]–[13] are described below:

### **1. Selective combining.**

The receiver keeps monitoring the SNR value of each diversity branch and selects the branch output with the largest SNR value as the received signal. It is the simplest diversity combining technique.

### **2. Maximal ratio combining.**

Since the selective combining technique uses only the selected branch and ignores the available information from all the other diversity branches, it is not optimum. The optimum linear combiner is called the maximal ratio combiner, in which the received signals at each branch are summed in a co-phased and weighted manner such that the highest achievable SNR is available at all times.

### **3. Equal-gain combining.**

In certain cases, it is not easy to provide for the variable channel amplitude gain required for the maximal ratio combining. An alternative approach is to set all the branch weights to unity after coherent detection and only provide equal gain combining diversity. In other words, the coherently detected signals from all the branches are simply added and applied to the decision device. Obviously, the complexity of this technique is lower than that of maximal ratio combining, but the performance is only marginally inferior to maximal ratio combining and superior to selection diversity.

## **1.2 Overview of Equalization Techniques**

The transmission of modulated signals over the multipath channel will be spread in time and cause intersymbol interference (ISI), which will distort the transmitted signal and cause bit errors at the receiver. In FDMA and TDMA systems, equalization is an effective way to combat the ISI in the received signal. Fig. 1.1 shows an equalized system, in which an effective channel is connected to an equalizer and a channel

estimator.

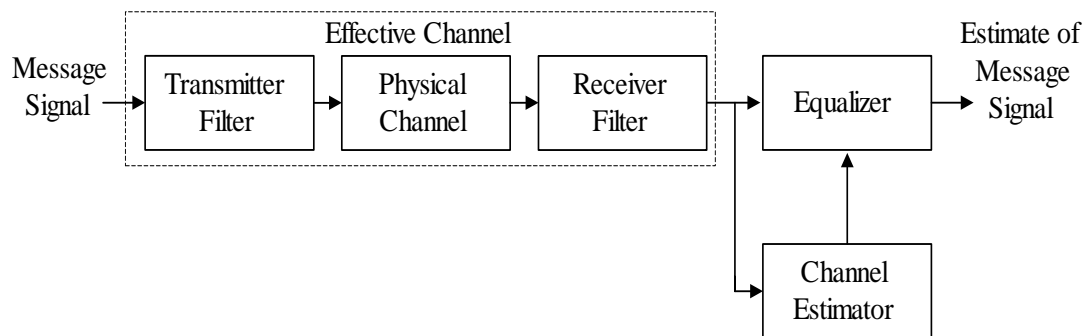


Fig. 1.1: An equalized system with a separate channel estimator.

Since a mobile radio channel is time varying, equalizers must be adaptive to track the variation of the channel. Four types of equalization techniques [14]–[16] are discussed below:

### 1. Maximum likelihood sequence estimation (MLSE) equalization.

This equalization technique calculates the Euclidian distances (metrics) between the sequence of the sampled received signal and all possible received sequences and determines the transmitted sequence with minimal distance. It is noteworthy that knowledge of the channel characteristics is necessary to compute the metrics for making decisions. The MLSE equalizer is optimum from a probability of error viewpoint. Unfortunately, its computation complexity grows exponentially with the length of channel time dispersion.

### 2. Linear equalization.

The linear transversal filters with adjustable filter coefficients are the most common used linear equalizers, for which the computation complexity is proportional to the length of channel time dispersion. Two criteria, the peak distortion criterion and the mean square error (MSE) criterion, are widely used to determine the filter coefficients.

1.) Peak distortion criterion: A receiver based on this criterion minimizes the

worst-case ISI (the peak distortion) at the equalizer output. In the case of an equalizer with an infinite number of taps, it is possible to determine a set of taps weights to force the peak distortion to zero. This means that the ISI is eliminated completely. This linear equalizer is simply an inverse filter of the channel and is also called a zero-forcing equalizer.

2.) MSE criterion: A receiver based on MSE criterion is constructed to minimize the mean square of the error signal between the equalized signal and the transmitted symbol. In contrast to the peak distortion criterion which does not take the channel noise into account, this criterion considers both ISI and channel noise. The minimum mean square error (MMSE) equalizer adjusts the tap weights of the equalizer in order to minimize the MSE, where the error includes the effects of both the ISI terms and the noise at the output of the equalizer.

### 3. Decision feedback equalization.

A linear equalizer is very effective in equalizing a channel for which ISI is not severe. In the case that a channel has spectral nulls in the passband (which is often encountered in wireless communications), a linear equalizer imposes high gain in the frequency domain to compensate for the spectral nulls and causes dramatic noise enhancement. To overcome this problem, nonlinear equalizers can be used. The decision feedback equalizer (DFE) is a nonlinear filter which consists of a feedforward filter and a feedback filter as shown in Fig. 1.2. The basic idea is to use previously detected symbols to eliminate the ISI in a feedback manner. As a result, the feedback filter does not cause the noise enhancement problem.

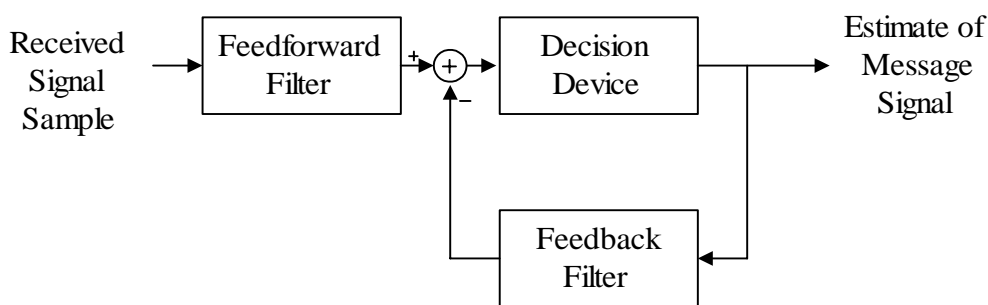


Fig. 1.2: The decision feedback equalizer.

#### 4. Turbo equalization.

Conventionally, an error control code (ECC) is used to protect data from errors that might occur in the transmission. An interleaver is used to randomize errors and avoid long error bursts. The concept of turbo equalization comes from turbo-codes and it combines a maximum a posteriori (MAP) equalizer with an MAP decoder through an iterative process [17]–[19]. In other words, turbo equalization is an iterative equalization and decoding technique for coded data transmission over a time dispersed channel. Fig. 1.3 shows a simplified block diagram of turbo equalization in which an iterative equalization and decoding loop is built based on the MAP criterion. Although turbo equalization can achieve near optimum BER performance for many transmission channels, it suffers from high computation complexity for channels with long memory and this high computation load is exacerbated as the iteration time increases. In addition, turbo equalization needs a perfect knowledge of the CIR. However, channel estimation could become very complicated due to the fact that turbo equalization scheme typically operates at low SNRs.

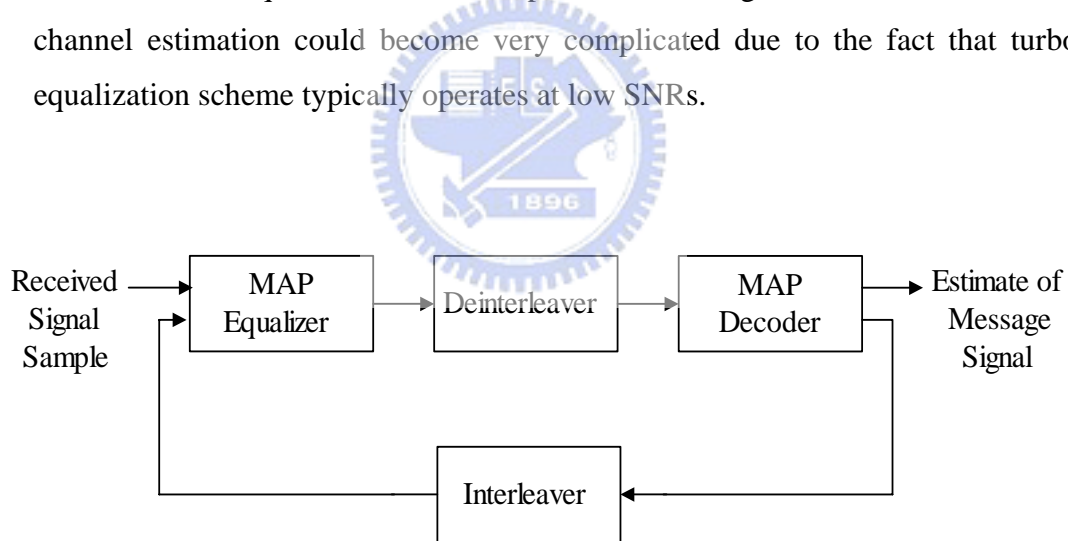


Fig. 1.3: A block diagram of turbo equalization.

### 1.3 Overview of Multi-user Detection Techniques

In direct sequence code division multiple system (DS/CDMA) systems, each user is assigned a different spreading code as a signature sequence. The cross correlations among the spreading codes are small. In addition, each user uses the entire frequency

band for transmission and all the users can transmit at the same time. The received signals of a DS/CDMA system are composed of the desired signal from the desired user and the interference signals from all the other users, which are referred to as the multiple access interference (MAI). MAI can be effectively suppressed by means of correlating the received signal with the desired user's spreading code, which can achieve a processing gain for suppressing MAI. However, the performance of the conventional single-user detection strategy drops significantly as the power of MAI becomes large. As a remedy, the multi-user detection (MUD) techniques make use of the detected data of multiple users to alleviate the MAI effects [20]–[21]. Note that the spreading codes of all users have to be known in advance and the objective of MUD techniques is to execute interference cancellation. Subtractive interference cancellation based MUD detectors are an important class of the multi-user detectors, and its basic idea is to reconstruct the interference signal contributed by each user in order to subtract out part or all of the MAI seen by each user. Such detectors are often implemented with multi-stages. The detector in each stage makes decision, regenerates and cancels out the MAI from the received signal. The hope is that the decisions will be improved at the output of successive stages. Based on similar concept, we can analogize the multipath interference in digital transmissions to MAI and use an MUD-like technique to improve the system performance in TDMA systems.

## 1.4 Overview of Channel Estimation Techniques

The wireless communication channels in mobile radio environments are usually multipath fading channels which result in ISI, and it can significantly increase transmission error rate. As a remedy, equalizers have been employed to alleviate the ISI effects. However, an accurate estimation of channel impulse response (CIR) is usually required in order to ensure successful equalization.

Consider a linear channel with CIR  $h(t)$ , real input  $x(t)$  and output  $y(t)$  as shown in Fig. 1.4, then we have [22]

$$R_{YX}(t) = R_{XX}(t) \otimes h(t) \quad (1.1)$$

where  $R_{YX}(t)$  denotes the cross-correlation function of  $y(t)$  and  $x(t)$ , and  $R_{XX}(t)$

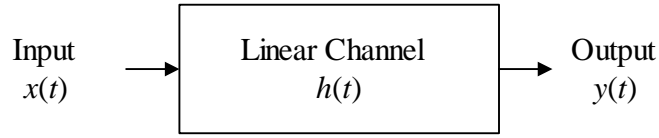


Fig. 1.4: A linear channel.

denotes the autocorrelation function of  $x(t)$ , and  $\otimes$  denotes the convolution operator. When the power spectrum of the input  $x(t)$  is white and its autocorrelation function  $R_{xx}(t)$  approaches the delta function  $\delta(t)$ , the cross-correlation function  $R_{yx}(t)$  is equal to the CIR  $h(t)$  approximately (i.e.,  $R_{yx}(t) \cong \delta(t) \otimes h(t) = h(t)$ ) [23]. That is, as the input  $x(t)$  is known, the CIR  $h(t)$  can be acquired through the cross-correlation of  $x(t)$  and  $y(t)$ . This is the original idea of most channel estimation techniques.

Channel estimation is normally done through transmitting a training sequence that is also known to the receiver. For the simplicity of implementation, most channel estimators usually use a correlation method to obtain the estimated CIR [24]–[28]. Since this method is executed by multiplying a central portion of the training sequence (called the normal training sequence) by different shifted versions of the received signal, it usually requires that a guard interval (a precursor and a postcursor) be added in the front and back portion of the training sequence, respectively. In addition, this correlation method requires that the normal training sequence has a good autocorrelation property in order to make an accurate CIR estimation. These limitations can be avoided by using the least-squares (LS) channel estimation method which requires only a precursor in the front portion of a training sequence and makes no assumption on good correlation property of the normal training sequence [26]–[28].

For reducing noise effects, an iterative channel estimation method has received great attention and has been proven effective [28]–[31]. This iterative channel estimation method was developed based on the idea that if the output of the equalizer can be used as an extended training sequence in the channel estimator, the quality of the channel estimation can be greatly improved. Obviously, a major restriction on the

iterative channel estimation method is that the decision errors of the equalizer output will be fed back to the channel estimator, known to as the error propagation, causing significantly degradation to system performance. In some extreme cases, such as in a fast fading environment, this method breaks down due to error propagation. In addition, the performance enhancement is obtained at the expense of an increase in implementation complexity and longer time delay due to hardware processing, which leads to difficulties in real time applications in practice. To alleviate the effects of error propagation, the iterative channel estimation method can be alternatively performed using the channel decoder output when the forward error correction coding has been taken into account [32], [33]. Nevertheless, the tremendous hardware complexity and more additional processing time further make this realization impractical.

## 1.5 Motivation for this Dissertation

A guard interval is usually added in the training sequence to keep the normal training sequence away from the multipath effects and the length of the guard interval should be greater than the maximum channel memory (or delay spread) of the channel. In a typical mobile radio communication environment, the effective multipath delays are usually much smaller than the length of the guard interval [34], [35]. For example, the root mean square (rms) delay spreads in the urban and hilly residential areas are 2-3 and 5  $\mu$ s, respectively, corresponding to about 1-2 bit periods for the GSM (Global System for Mobile Communications) system in which the guard interval setting is 5 bits. This implies that most bits in the guard interval might not be affected by ISI, which are called here as the uncorrupted data and are available for estimating the CIR. This suggests that an improved channel estimation method can be developed based on both the uncorrupted data and the normal training sequence.

In order to fully utilize all the useful information in the guard interval, two types of two-stage channel estimation methods are proposed: the least-squares based two-stage channel estimation (LS-2SCE) method and the multipath interference cancellation based two-stage channel estimation (MIC-2SCE) method. Both methods execute a conventional channel estimation method based on the normal training sequence to obtain a coarse CIR in the first stage. The corresponding results were

used to estimate both the maximum channel memory and the effective paths, and then to locate the uncorrupted data in the guard interval. The uncorrupted data together with the normal training sequence, referred to as an extended normal training sequence, could be used to enhance the performance in the channel estimation.

In the LS-2SCE method, the LS algorithm was performed again on the extended normal training sequence to obtain the fine-tuned CIR in the second stage. Since more useful data can be used in the second stage, the estimation performance can be improved.

In order to reduce the computation complexity, the MIC-2SCE method is proposed to replace the LS algorithm in the second stage of the LS-2SCE method. Since the training sequence was already known in the receiver, and both the maximum channel memory and the effective paths were obtained in the first stage, the multipath interference cancellation (MIC) algorithm, which is similar to the subtractive interference cancellation method in MUD of CDMA systems [20], [36]–[38], could be executed on the extended normal training sequence to extract the individual path signal. As a result, the correlation method could be used to obtain the fine-tuned CIR in the second stage.

Since the multipath phenomenon in the radio channel provides multiple versions of original transmitted signal at a receiver. If the individual path components can be separated and gathered back together through optimal linear combining, the SNR would be increased and therefore the reliability of data reception can be improved. In other words, if the individual path components in multipath channel can be separated, they can be utilized to achieve path diversity. In CDMA systems, the multipath interference can be suppressed by the processing gain, and the multipath diversity can be efficiently achieved by using a RAKE receiver. However, there are no spreading codes used in TDMA systems. Therefore, the multipath interference cannot be suppressed and the individual path signal cannot be extracted. Nevertheless, we can treat each individual path as a single user and the multipath interference as MAI. Then the individual path components can be separated by using an MIC method if we can get known data and the information of CIR.

In order to achieve implicit multipath diversity in TDMA systems, a posterior

block iterative decision feedback detector is proposed to enhance the performance of a conventional detector (or equalizer) in this dissertation. Using a conventional detector as a preliminary detector, the preliminary decided data and estimated CIR can be obtained. Jointly using these results, we can use the MIC algorithm to remove the multipath interference and to extract the individual path signal. In other words, a means for reducing ISI is devised. Then the maximal-ratio combining (MRC) technique can be used to combine these signals to increase the SNR of the system and therefore achieve more reliable data detection. Furthermore, the more reliably detected data can be feedback to the posterior detector to improve the system performance again in an iterative manner.

## 1.6 Organization of this Dissertation

This dissertation presents two channel estimation methods and a posterior block iterative decision feedback detector for digital wireless communication systems. The subjects covered in the following chapters are organized as:

In Chapter 2, the proposed LS-2SCE method is described. Both theoretical analysis and computer simulations were done to verify the efficiency of the proposed method.

In Chapter 3, the proposed MIC-2SCE method is described. Theoretical analysis, computer simulations, and a discussion on computation complexity were done to verify the efficiency and the feasibility of the proposed method.

In Chapter 4, the proposed posterior block iterative decision feedback detector is described. Computer simulations were done in both static and fading multipath channels to verify its performance enhancement in BER.

In Chapter 5, a conclusion of this dissertation and a discussion on future research directions are given.

# Chapter 2

## A Least-squares Based Two-stage Channel Estimation Method

### 2.1 Introduction

The radio channels in digital wireless communications usually are multipath fading channels, which generate intersymbol interference (ISI) in the received signal that may cause serious performance degradation. To alleviate the ISI effects, equalizers are commonly employed and they usually require an accurate estimate of channel impulse response (CIR) in order to ensure successful equalization.

Conventionally, CIR is estimated based on a known training sequence, which is sent by the transmitter and is repeated in every transmitted data burst. A guard interval included in the training sequence is used to keep the normal training sequence away from the ISI caused by the adjacent random data. Since the length of the guard interval in a communication system should be large than the maximum channel memory in all possible radio propagation environments, the effective multipath delay is usually much smaller than the length of guard interval in practice [34], [35]. This suggests that the uncorrupted data in the guard interval can be employed to improve the channel estimation accuracy.

In order to fully utilize all the useful information in the guard interval, a novel least-squares based two-stage channel estimation (LS-2SCE) method is proposed in this chapter. In the first stage, a least-squares (LS) algorithm [39] was used to estimate

the CIR based on the normal training sequence. In order to determine the maximum channel memory, the weaker paths with strength less than a certain threshold  $\theta$  were discarded. The threshold  $\theta$  was defined as a small factor of the strongest amplitude of all estimated paths. After the maximum channel memory was estimated, it was used to locate the uncorrupted data in the guard interval. In the second stage, the uncorrupted data together with the normal training sequence were sent to the LS algorithm again to obtain the fine-tuned CIR. Since more bits were utilized for channel estimation, the proposed method led to an improved performance compared to conventional methods. To verify the efficiency of the proposed LS-2SCE method, both a theoretical analysis and computer simulations have been done. Our computer simulation results confirm the analysis results and demonstrate that the proposed LS-2SCE method really outperforms a conventional single-stage channel estimation method.

This chapter describes the operation principles, conducts the theoretic analysis and evaluates the performance of the proposed LS-2SCE method. In Section 2.2, both the system model and the conventional channel estimation methods are described. In Section 2.3, the details of the proposed LS-2SCE method including the function of each stage and the algorithms used are presented. In Section 2.4, theoretic analysis on the LS-2SCE method is given. Computer simulation results are presented in Section 2.5. Finally, a conclusion is given in Section 2.6.

## 2.2. The System Model and Conventional Channel Estimation Methods

The scenario considered here involves a digital communications system in a multipath channel which consists of  $L$  paths. In the receiving end, the received baseband signal at a certain sampling instant can be expressed as

$$r[m] = \sum_{k=0}^{L-1} h[k]d[m-k] + n[m] \quad (2.1)$$

where  $d[m]$  is the transmitted data symbol and  $h[k]$  denotes the complex gain associated with the  $k$ th path. It is noteworthy that the  $L$  complex gains and their

corresponding delays determine the overall CIR and  $n[m]$  is the additive white Gaussian noise (AWGN) with zero mean and variance  $\sigma_n^2$ . A conventional channel estimation method is usually based on a known training sequence [8], e.g., the midamble of the transmitted data burst in the GSM system, the preamble in the IEEE 802.11a wireless local area network standard and the pilot tones in the DVB (Digital Video Broadcasting) system [40], [41].

A guard interval is typically generated from the cyclic extension of the normal training sequence [42], [43]. Without loss of generality, let a binary normal training sequence be denoted as  $\{s_0, s_1, \dots, s_{N-1}\}$ , where  $s_i \in \{1, -1\}$ . Including a cyclically extended prefix, the transmitted training sequence is then given by  $\{s_{N-M}, s_{N-M+1}, \dots, s_{N-1}, s_0, s_1, \dots, s_{N-1}\}$ , where  $M$  is the length of the guard interval and  $M \geq L - 1$ . The training sequence is depicted in Fig. 2.1. Note that the training sequence can be divided into the  $N$ -bit normal training sequence portion which is used by conventional channel estimation methods and the  $M$ -bit prefix portion (guard interval). These prefix bits might be corrupted from the data bits transmitted in front due to the multipath effects introduced by the radio environment.

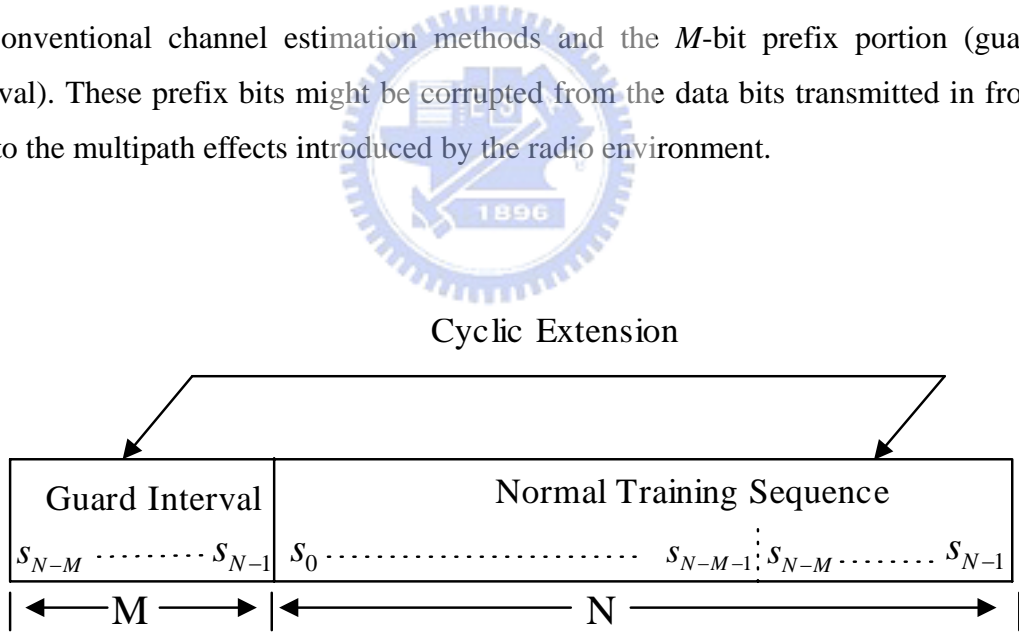


Fig. 2.1: The guard interval and the normal training sequence of the training sequence.

The received signal associated with the normal training sequence can be expressed in an  $N \times 1$  vector  $\mathbf{r}_t$  as given by

$$\mathbf{r}_t = \mathbf{S}\mathbf{h} + \mathbf{n} \quad (2.2)$$

where the complex CIR vector  $\mathbf{h} = [h_0 \ h_1 \ \cdots \ h_{L-1}]^T$  with  $T$  denoting the transpose operator, and the  $N \times 1$  vector  $\mathbf{n}$  denotes the noise samples. The  $N \times L$  normal training sequence matrix  $\mathbf{S}$  is then given by

$$\mathbf{S} = \begin{bmatrix} s_0 & s_{N-1} & \cdots & s_{N-L+1} \\ s_1 & s_0 & \cdots & s_{N-L+2} \\ \vdots & \vdots & \ddots & \vdots \\ s_{N-1} & s_{N-2} & \cdots & s_{N-L} \end{bmatrix} \quad (2.3)$$

The goal of a conventional LS channel estimator is to find an estimate of  $\mathbf{h}$  in order to minimize the sum of squared error between the received data and the reconstructed data, which can be written as

$$\min_{\mathbf{h}_{ls}} \|\mathbf{r}_t - \mathbf{S}\mathbf{h}_{ls}\|^2 \quad (2.4)$$

where  $\|\cdot\|$  denotes the 2-norm operator. The optimum solution of this cost function is [44]

$$\hat{\mathbf{h}}_{ls} = (\mathbf{S}^H \mathbf{S})^{-1} \mathbf{S}^H \mathbf{r}_t \quad (2.5)$$

where  $(\cdot)^{-1}$  and  $H$  denote the matrix inverse and Hermitian operations, respectively. The above solution, referred to as the LS channel estimation, has been shown to be the best linear unbiased estimate of the CIR [45]. A normal training sequence is said to be perfect if its associated correlation matrix  $\mathbf{S}^H \mathbf{S}$  is diagonal and the mean squared channel estimation error can be minimized [46]. This holds for the 16-bit normal training sequences of GSM, which is in the central part of a midamble of 26 bits. In this case, the solution in (2.5) can be further simplified to

$$\hat{\mathbf{h}}_{ls} = \alpha \mathbf{S}^H \mathbf{r}_t \quad (2.6)$$

where  $\alpha$  is a scaling constant. The simplified channel estimator can be obtained by correlating the received signal with the normal training sequence. In this case, the LS channel estimation method is the same as the correlation channel estimation method. For simplicity and consistency, hereafter, this chapter uses the term Conv-CE method to denote the conventional LS channel estimation method based on the normal

training sequence.

## 2.3 The Proposed LS-2SCE Method

A flow chart of the proposed LS-2SCE method is shown in Fig. 2.2. The details of the proposed LS-2SCE method are described below:

### 2.3.1 The first stage

As shown in Fig. 2.2, the purpose of the first stage channel estimation is to find the maximum channel memory  $K$ . Therefore, an initial estimation of CIR can be obtained by executing the Conv-CE method. As we mentioned above, if the correlation matrix  $\mathbf{S}^H \mathbf{S}$  is diagonal, the Conv-CE method can be reduced to the correlation channel estimation method.

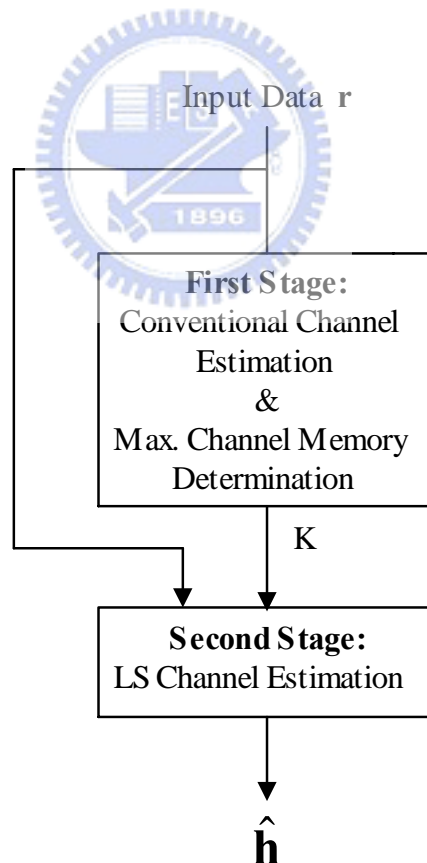


Fig. 2.2: A flow chart of the proposed LS-2SCE method

After obtaining the initial CIR estimation, the strongest path among all the

estimated paths is selected as the reference path and its amplitude is denoted as  $A_{\max}$ . All the paths whose amplitude (normalized by  $A_{\max}$ ) smaller than a threshold  $\theta$  are discarded. The threshold  $\theta$  is a system parameter and is a small factor of  $A_{\max}$  [47], [48].

Following the above selection procedure, only effective paths remain in the initially estimated CIR. Accordingly, the last effective path needs to be found and its position is located. If the location of the first path is set to 0, the maximum channel memory  $K$ , is set to the location of the last effective path.

### 2.3.2 The second stage

After the maximum channel memory  $K$  is estimated in the first stage, it can be used to locate the  $M - K$  uncorrupted data in the guard interval, which can be utilized to improve the performance of channel estimation in the second stage.

In matrix notation, the  $(N + M - K) \times 1$  extended received signal vector  $\mathbf{r}_{aug}$  associated with the  $M - K$  uncorrupted bits plus the normal training sequence of length  $N$  is given by

$$\mathbf{r}_{aug} = \mathbf{S}_tr \mathbf{h} + \mathbf{n} \quad (2.7)$$

where the  $(N + M - K) \times L$  vector  $\mathbf{S}_tr$  consists of the transmitted data and the  $(N + M - K) \times 1$  vector  $\mathbf{n}$  denotes the noise samples. Let us define an  $(N + M - K) \times L$  augmentation matrix  $\mathbf{S}_{aug}$  which is composed of the training sequence and express it in terms of the normal training sequence matrix  $\mathbf{S}$  as below

$$\mathbf{S}_{aug} = \begin{bmatrix} s_{N-M+K} & s_{N-M+K-1} & \cdots & s_{N-M+K-L+1} \\ s_{N-M+K+1} & s_{N-M+K} & \cdots & s_{N-M+K-L+2} \\ \vdots & \vdots & \ddots & \vdots \\ s_{N-1} & s_{N-2} & \cdots & s_{N-L} \\ s_0 & s_{N-1} & \cdots & s_{N-L+1} \\ s_1 & s_0 & \cdots & s_{N-L+2} \\ \vdots & \vdots & \ddots & \vdots \\ s_{N-1} & s_{N-2} & \cdots & s_{N-L} \end{bmatrix} = \begin{bmatrix} \mathbf{G}_{(M-K) \times N} \\ \mathbf{I}_N \end{bmatrix} \mathbf{S} \quad (2.8)$$

where  $\mathbf{G} = \begin{bmatrix} \mathbf{O}_{(M-K) \times (N-M+K)} & \mathbf{I}_{(M-K)} \end{bmatrix}$  is a selection matrix which is used to extract the uncorrupted data in the guard interval corresponding to the normal training sequence matrix  $\mathbf{S}$ ;  $\mathbf{I}$  and  $\mathbf{O}$  denote identity matrix and null matrix, respectively.

The matrix  $\mathbf{S}_{tr}$  can be represented by  $\mathbf{S}_{aug}$  plus an error matrix  $\mathbf{\Delta}$  and (2.7) can be rewritten as

$$\mathbf{r}_{aug} = (\mathbf{S}_{aug} + \mathbf{\Delta})\mathbf{h} + \mathbf{n} \quad (2.9)$$

where the  $(N + M - K) \times L$  error matrix  $\mathbf{\Delta}$  denotes the difference between the matrix  $\mathbf{S}_{tr}$  and the matrix  $\mathbf{S}_{aug}$  (i.e.,  $\mathbf{\Delta} = \mathbf{S}_{tr} - \mathbf{S}_{aug}$ ). Most elements in matrix  $\mathbf{\Delta}$  are null except those lie in the small upper right triangular region of the matrix. Since all these nonzero elements in matrix  $\mathbf{\Delta}$  are multiplied by the corresponding weaker paths which is in vector  $\mathbf{h}$  in the product  $\mathbf{\Delta}\mathbf{h}$ . When the threshold  $\theta$  in stage 1 is set small enough, the paths discarded are very weak and the corresponding values in the residual vector  $\mathbf{\Delta}\mathbf{h}$  are also very small. Neglecting the effect of the residue vector  $\mathbf{\Delta}\mathbf{h}$ , (2.9) can be approximately written as

$$\mathbf{r}_{aug} \approx \mathbf{S}_{aug}\mathbf{h} + \mathbf{n} \quad (2.10)$$

Therefore, the goal of the second stage LS channel estimation is to find  $\mathbf{h}$  which achieves

$$\min_{\mathbf{h}_{2s}} \|\mathbf{r}_{aug} - \mathbf{S}_{aug}\mathbf{h}_{2s}\|^2 \quad (2.11)$$

Accordingly, the LS solution is given by

$$\hat{\mathbf{h}}_{2s} = (\mathbf{S}_{aug}^H \mathbf{S}_{aug})^{-1} \mathbf{S}_{aug}^H \mathbf{r}_{aug} \quad (2.12)$$

Although both (2.5) and (2.12) are needed in the proposed LS-2SCE method and matrix inverse operations are required, the computation is simple because both the matrix  $\mathbf{S}$  and the matrix  $\mathbf{S}_{aug}$  are only functions of the known training sequence, and the matrix inverse operations can be computed and stored in advance.

The algorithm of the proposed LS-2SCE method is summarized as follows:

### Stage I.

1. Set the system parameters: the maximum CIR length  $L$  and the threshold  $\theta$ .
2. Obtain an initially estimated CIR  $\hat{\mathbf{h}}_{1s}$ , according to (2.5).
3. Find the strongest path:  $A_{\max} = \max(|h_i|)$  for  $i = 0, 1, \dots, L-1$ .
4. Set the negligible path to zero: If  $(|h_i|/A_{\max}) < \theta$ , then let  $h_i = 0$  for  $i = 0, 1, \dots, L-1$ .
5. Find the last nonzero path:  $h_i$  for  $0 \leq i \leq L-1$ . Then, set the maximum channel memory  $K = i$ .

### Stage II.

1. Use the parameter  $K$  to get the augmentation matrix  $\mathbf{S}_{aug}$ .
2. Obtain a finally estimated CIR  $\hat{\mathbf{h}}_{2s}$ , according to (2.12).

## 2.4 Performance Analysis

In this section, a theoretical analysis is given to verify that the performance of the proposed LS-2SCE method is superior to the Conv-CE method.

According to the optimum solution in (2.5), the corresponding mean square error (MSE) of the conventional LS channel estimator is given by [44]

$$MSE_{conv} = \sigma_n^2 \text{tr}\left\{(\mathbf{S}^H \mathbf{S})^{-1}\right\} \quad (2.13)$$

where  $\text{tr}(\cdot)$  denotes the trace operator and  $\sigma_n^2$  denotes the input noise power. Applying the singular value decomposition (SVD) technique [49] to the normal training sequence matrix  $\mathbf{S}$  yields

$$\mathbf{S} = \mathbf{U} \begin{bmatrix} \boldsymbol{\Sigma} \\ \mathbf{O} \end{bmatrix} \mathbf{V}^H \quad (2.14)$$

where  $\mathbf{\Sigma}$  denotes an  $L \times L$  diagonal matrix formed by the singular values of matrix  $\mathbf{S}$ ;  $\mathbf{O}$  denotes an  $(N - L) \times L$  null matrix, and both the  $N \times N$  matrix  $\mathbf{U}$  and the  $L \times L$  matrix  $\mathbf{V}$  are unitary. Substituting (2.14) into (2.13), the MSE of the Conv-CE method becomes

$$\begin{aligned}
MSE_{conv} &= \sigma_n^2 \text{tr} \left\{ \left( \mathbf{V} \begin{bmatrix} \mathbf{\Sigma} & \mathbf{O} \end{bmatrix} \mathbf{U}^H \mathbf{U} \begin{bmatrix} \mathbf{\Sigma} \\ \mathbf{O} \end{bmatrix} \mathbf{V}^H \right)^{-1} \right\} \\
&= \sigma_n^2 \text{tr} \left\{ \left( \mathbf{V} \mathbf{\Sigma}^2 \mathbf{V}^H \right)^{-1} \right\} \\
&= \sigma_n^2 \text{tr} \left\{ \mathbf{\Sigma}^{-2} \right\} \\
&= \sigma_n^2 \sum_{i=1}^L \lambda_i^{-1}
\end{aligned} \tag{2.15}$$

where  $\lambda_i$  for  $i=1,2,\dots,L$  are the eigenvalues of the correlation matrix  $\mathbf{S}^H \mathbf{S}$ . Since the matrix  $\mathbf{S}^H \mathbf{S}$  is positive semidefinite [50], its eigenvalues are nonnegative.

The following analysis of the proposed LS-2SCE method is based on the assumption that the paths discarded are very weak. When the residual vector  $\mathbf{\Delta} \mathbf{h}$  is relatively small compared with the noise, it can be neglected and equality in (2.10) holds. Replacing  $\mathbf{S}$  with  $\mathbf{S}_{aug}$  in (2.13) and expressing  $\mathbf{S}_{aug}$  in terms of  $\mathbf{S}$  as given in (2.8), the MSE of the LS-2SCE method can be expressed as

$$\begin{aligned}
MSE_{2S} &= \sigma_n^2 \text{tr} \left\{ \left( \mathbf{S}_{aug}^H \mathbf{S}_{aug} \right)^{-1} \right\} \\
&= \sigma_n^2 \text{tr} \left\{ \left( \mathbf{S}^H \begin{bmatrix} \mathbf{G}^H & \mathbf{I} \end{bmatrix} \begin{bmatrix} \mathbf{G} \\ \mathbf{I} \end{bmatrix} \mathbf{S} \right)^{-1} \right\} \\
&= \sigma_n^2 \text{tr} \left\{ \left[ \mathbf{S}^H \left( \mathbf{I} + \mathbf{G}^H \mathbf{G} \right) \mathbf{S} \right]^{-1} \right\}
\end{aligned} \tag{2.16}$$

Assuming the signal power is normalized to unity, (2.13) and (2.16) indicate that in dB scale both  $MSE_{conv}$  and  $MSE_{2S}$  decrease linearly as SNR increase.

In the case of  $M - K = 0$ , there is no uncorrupted data in the guard interval and the correlation matrix  $\mathbf{G}^H \mathbf{G} = \mathbf{O}$ . The result of  $MSE_{2s} = MSE_{conv}$  can be obtained from (2.13) and (2.16). In the case of  $M - K = N$ , there are  $N$  bits uncorrupted data in the guard interval and the correlation matrix  $\mathbf{G}^H \mathbf{G} = \mathbf{I}$ . The result of  $MSE_{2s} = \frac{1}{2} MSE_{conv}$  can be obtained from (2.13) and (2.16).

Substituting (2.14) into (2.16) yields

$$\begin{aligned}
MSE_{2s} &= \sigma_n^2 tr \left\{ \left( \mathbf{V} \begin{bmatrix} \boldsymbol{\Sigma} & \mathbf{O} \end{bmatrix} \mathbf{U}^H (\mathbf{G}^H \mathbf{G} + \mathbf{I}) \mathbf{U} \begin{bmatrix} \boldsymbol{\Sigma} \\ \mathbf{O} \end{bmatrix} \mathbf{V}^H \right)^{-1} \right\} \\
&= \sigma_n^2 tr \left\{ \left( \mathbf{V} \begin{bmatrix} \boldsymbol{\Sigma} & \mathbf{O} \end{bmatrix} \mathbf{U}^H \mathbf{G}^H \mathbf{G} \mathbf{U} \begin{bmatrix} \boldsymbol{\Sigma} \\ \mathbf{O} \end{bmatrix} \mathbf{V}^H + \mathbf{V} \begin{bmatrix} \boldsymbol{\Sigma} & \mathbf{O} \end{bmatrix} \mathbf{U}^H \mathbf{I} \mathbf{U} \begin{bmatrix} \boldsymbol{\Sigma} \\ \mathbf{O} \end{bmatrix} \mathbf{V}^H \right)^{-1} \right\} \\
&= \sigma_n^2 tr \left\{ \left( \mathbf{V} \begin{bmatrix} \boldsymbol{\Sigma} & \mathbf{O} \end{bmatrix} \mathbf{U}^H \mathbf{G}^H \mathbf{G} \mathbf{U} \begin{bmatrix} \boldsymbol{\Sigma} \\ \mathbf{O} \end{bmatrix} \mathbf{V}^H + \mathbf{V} \begin{bmatrix} \boldsymbol{\Sigma} & \mathbf{O} \end{bmatrix} \begin{bmatrix} \boldsymbol{\Sigma} \\ \mathbf{O} \end{bmatrix} \mathbf{V}^H \right)^{-1} \right\} \\
&= \sigma_n^2 tr \left\{ \left( \mathbf{V} \begin{bmatrix} \boldsymbol{\Sigma} & \mathbf{O} \end{bmatrix} \mathbf{U}^H \mathbf{G}^H \mathbf{G} \mathbf{U} \begin{bmatrix} \boldsymbol{\Sigma} \\ \mathbf{O} \end{bmatrix} \mathbf{V}^H + \mathbf{V} \boldsymbol{\Sigma}^2 \mathbf{V}^H \right)^{-1} \right\} \tag{2.17}
\end{aligned}$$

Let us further partition the unitary matrix  $\mathbf{U}$  into four matrices as given by

$$\mathbf{U} = \begin{bmatrix} \mathbf{W}_{(N-M+K) \times L} & \mathbf{X}_{(N-M+K) \times (N-L)} \\ \mathbf{Z}_{(M-K) \times L} & \mathbf{Y}_{(M-K) \times (N-L)} \end{bmatrix} \tag{2.18}$$

such that

$$\mathbf{G} \mathbf{U} \begin{bmatrix} \boldsymbol{\Sigma} \\ \mathbf{O} \end{bmatrix} = \begin{bmatrix} \mathbf{O} & \mathbf{I} \end{bmatrix} \mathbf{U} \begin{bmatrix} \boldsymbol{\Sigma} \\ \mathbf{O} \end{bmatrix} = \mathbf{Z} \boldsymbol{\Sigma} \tag{2.19}$$

Substituting (2.19) into (2.17) and performing some matrix operations, we get

$$MSE_{2s} = \sigma_n^2 tr \left\{ \mathbf{V} \boldsymbol{\Sigma}^{-1} (\mathbf{I} + \mathbf{Z}^H \mathbf{Z})^{-1} \boldsymbol{\Sigma}^{-1} \mathbf{V}^H \right\}$$

$$= \sigma_n^2 \text{tr} \left\{ \boldsymbol{\Sigma}^{-2} (\mathbf{I} + \mathbf{Z}^H \mathbf{Z})^{-1} \right\} \quad (2.20)$$

Applying the SVD technique again to the  $(M-L) \times L$  matrix  $\mathbf{Z}$  yields

$$\mathbf{Z} = \tilde{\mathbf{U}} \begin{bmatrix} \tilde{\boldsymbol{\Sigma}} \\ \mathbf{O} \end{bmatrix} \tilde{\mathbf{V}}^H \quad (2.21)$$

where  $\tilde{\boldsymbol{\Sigma}}$  denotes an  $L \times L$  diagonal matrix formed by the singular values of matrix  $\mathbf{Z}$ ;  $\mathbf{O}$  denotes an  $(M-K-L) \times L$  null matrix, and both the  $(M-L) \times (M-L)$  matrix  $\tilde{\mathbf{U}}$  and the  $L \times L$  matrix  $\tilde{\mathbf{V}}$  are unitary. Substituting (2.21) into the autocorrelation matrix

$$\mathbf{Z}^H \mathbf{Z} = \tilde{\mathbf{V}} \begin{bmatrix} \tilde{\boldsymbol{\Sigma}} & \mathbf{O} \end{bmatrix} \tilde{\mathbf{U}}^H \tilde{\mathbf{U}} \begin{bmatrix} \tilde{\boldsymbol{\Sigma}} \\ \mathbf{O} \end{bmatrix} \tilde{\mathbf{V}}^H = \tilde{\mathbf{V}} \tilde{\boldsymbol{\Sigma}}^2 \tilde{\mathbf{V}}^H = \tilde{\mathbf{V}} \mathbf{D} \tilde{\mathbf{V}}^H \quad (2.22)$$

where  $\mathbf{D}$  is a diagonal matrix with diagonal eigenvalue elements  $\tilde{\lambda}_i$   $i=1,2,\dots,L$ . Substituting (2.22) into (2.20), the MSE of the LS-2SCE method can be rewritten as

$$\begin{aligned} MSE_{2s} &= \sigma_n^2 \text{tr} \left\{ \boldsymbol{\Sigma}^{-2} (\mathbf{I} + \tilde{\mathbf{V}} \mathbf{D} \tilde{\mathbf{V}}^H)^{-1} \right\} \\ &= \sigma_n^2 \text{tr} \left\{ \boldsymbol{\Sigma}^{-2} (\tilde{\mathbf{V}} \tilde{\mathbf{V}}^H + \tilde{\mathbf{V}} \mathbf{D} \tilde{\mathbf{V}}^H)^{-1} \right\} \\ &= \sigma_n^2 \text{tr} \left\{ \boldsymbol{\Sigma}^{-2} \tilde{\mathbf{V}} (\mathbf{I} + \mathbf{D})^{-1} \tilde{\mathbf{V}}^H \right\} \\ &= \sigma_n^2 \text{tr} \left\{ \boldsymbol{\Sigma}^{-2} \begin{bmatrix} \tilde{\mathbf{v}}_1^H \\ \vdots \\ \tilde{\mathbf{v}}_L^H \end{bmatrix} (\mathbf{I} + \mathbf{D})^{-1} [\tilde{\mathbf{v}}_1 \quad \dots \quad \tilde{\mathbf{v}}_L] \right\} \\ &= \sigma_n^2 \sum_{i=1}^L \lambda_i^{-1} \tilde{\mathbf{v}}_i^H (\mathbf{I} + \mathbf{D})^{-1} \tilde{\mathbf{v}}_i \\ &= \sigma_n^2 \sum_{i=1}^L \lambda_i^{-1} \left\| (\mathbf{I} + \mathbf{D})^{-\frac{1}{2}} \tilde{\mathbf{v}}_i \right\|^2 \end{aligned} \quad (2.23)$$

where  $\tilde{\mathbf{v}}_i^H$  is the  $i$ th row of the unitary matrix  $\tilde{\mathbf{V}}$ .

Since the matrix  $\mathbf{Z}^H \mathbf{Z}$  is positive semidefinite, its eigenvalues  $\tilde{\lambda}_i$  for  $i=1,2,\dots,L$  are nonnegative and the diagonal elements of  $(\mathbf{I} + \mathbf{D})^{-1}$  are equal or less than one. It follows that

$$MSE_{2S} \leq \sigma_n^2 \sum_{i=1}^L \lambda_i^{-1} \|\tilde{\mathbf{v}}_i\|^2 = \sigma_n^2 \sum_{i=1}^L \lambda_i^{-1} = MSE_{conv} \quad (2.24)$$

indicating that the proposed LS-2SCE method outperforms the Conv-CE method.

## 2.5 Computer Simulations

To evaluate the performance of the proposed LS-2SCE method, a series of computer simulations were carried out under different channel conditions. In order to compare the performance of different channel estimators, the normalized MSE between the ideal CIR vector,  $\mathbf{h}$ , and the estimated CIR vector,  $\hat{\mathbf{h}}$ , was defined as

$$MSE = E \left\{ \|\mathbf{h} - \hat{\mathbf{h}}\|^2 \right\} / E \left\{ \|\mathbf{h}\|^2 \right\} \quad (2.25)$$

where  $E\{\cdot\}$  denotes the expectation operator.

Our simulations were divided into two parts. In the first part, the general behavior of the LS-2SCE method was investigated in a multipath environment. In the second part, the data burst of GSM was employed to examine the performances of the LS-2SCE method in both a two-path fixed channel and a two-path fading channel. As a comparison, the corresponding results of the Conv-CE method were also included.

In all our simulations, the power of the CIR vector was normalized to one. The maximum CIR length  $L$  was set to 6 and the binary phase shift keying (BPSK) modulation method was assumed.

### 2.5.1 Part 1: General behavior of the proposed channel estimator

In the first part of our simulations, the input SNR was set to 15 dB and the length of the normal training sequence was set to 20. The training sequence was randomly generated such that it constructs a full rank normal training sequence matrix  $\mathbf{S}$ . The analysis result of the LS-2SCE method calculated from (2.16) is plotted as a dashed

line in each figure.

To investigate the effect of the guard interval length on channel estimation in an equal-gain two-path fixed channel, the first path was set at the 1st sample, the second path was set at the 2nd sample, and the guard interval length was varied from 7 to 21. The threshold  $\theta$  used in the first stage was set to  $-15$  dB relative to the strongest amplitude of all the estimated paths. The corresponding MSE versus the ratio of the length of the uncorrupted data to the length of the normal training sequence is shown in Fig. 2.3. This ratio,  $(M - K)/N$ , is referred to as the excess length ratio. It is observed that the MSE of the simulated LS-2SCE method is close to the analysis result and it decreases as the excess length ratio increases. This is because that the length of the uncorrupted data increases as the guard interval length increases. On the contrary, the MSE of the Conv-CE method is approximately a constant due to the fixed length of the normal training sequence. Note that the MSE ratio of the Conv-CE method to the LS-2SCE is close to 2 when the excess length ratio is 1. This result is consistent with our analysis result. In this case, the MSE of the LS-2SCE method is approximate 3 dB less than that of the Conv-CE method.

To evaluate the effect of the maximum channel memory on the performance of the LS-2SCE method, the guard interval length was set to 10, and an equal-gain two-path channel was modeled in such a way that the first path was fixed at the 1st sample and the second path was changed from the 2nd sample to  $L$ th sample. The threshold  $\theta$  was set to  $-15$  dB. The corresponding MSE versus the variation in maximum channel memory is shown in Fig. 2.4. It is observed that the MSE of the LS-2SCE method is close to the analysis result and increases as the maximum channel memory increases. This is because that fewer bits are used for channel estimation in the LS-2SCE method as the maximum channel memory increases.

To examine the effect of weaker paths on the performance of the LS-2SCE method, the guard interval length was again set to 10, and a channel with two strong paths of equal power followed by four weaker paths also of equal power was employed in the simulation. The amplitudes of strong paths were set to 1 and the amplitudes of weaker paths were varied from 0 to 0.25. The corresponding MSE versus different amplitudes of the four weaker paths under two different SNRs and threshold  $\theta$  s is shown in Fig. 2.5. It is observed that the analysis result is consistent

with the simulation result when the amplitudes are small. However, as the amplitudes begin to increase, the residual vector  $\Delta \mathbf{h}$  in (2.9) becomes significant and this leads to a performance degradation in MSE. Gradually, when the amplitudes (normalized by  $A_{\max}$ ) are larger than the threshold, the weaker paths will be taken in and considered as effective paths. Finally, all weaker paths are retained and the maximum value of  $K$  is obtained. In this case, the corresponding MSE becomes a constant. It is noteworthy that the MSE curves in the SNR =13 dB case are smoother as compared with those obtained in the SNR=18 dB case. This is because that the effect of noise is more significant than the effect of the residual vector  $\Delta \mathbf{h}$  in (2.9) at a lower SNR. Furthermore, to clarify the combined effect of weaker paths and the threshold, we simulated the cases of amplitudes of weaker paths being equal to 0, 0.1, and 0.25 respectively. Fig. 2.6 shows that only in the case of weaker path amplitude = 0.25, and when the threshold is improperly chosen ( $>-10$  dB), the performance of MSE will significantly degrade. This is because that the weaker paths were discarded at a high threshold  $\theta$  value and this causes the effect of residual vector  $\Delta \mathbf{h}$  more significant. Therefore, a small value of threshold is suggested to use in practice. As a rule of thumb, the threshold  $\theta$  can be approximately chosen as a  $-\text{SNR}$  (dB) value such that the performance improvement can be assured.

## 2.5.2 Part 2: Performance Enhancement with the Proposed Channel Estimator

In the second part of our simulations, the GSM burst structure with a GSM midamble 00100101110000100010010111 as defined by ETSI (European Telecommunications Standards Institute) [25] was employed, and the BPSK modulation method was simulated at a data rate of 270.833 kbit/sec. When the GSM midamble is mapped into the structure of Fig. 2.1, it can be separated into a 10-bit guard interval and a 16-bit normal training sequence. The threshold  $\theta$  was set to  $-15$  dB in the following simulations.

To illustrate the performance of the LS-2SCE method in an equal-gain two-path fixed channel, the first path was located at the 1st sample, the second path was randomly located from the 2nd to the  $L$ th sample, and the SNR was varied from 10 to 20 dB. The corresponding results are shown in Fig. 2.7. This figure shows that the

MSE of the LS-2SCE method is close to the analysis result, which is calculated from (2.16) and is plotted as a dashed line. This figure also shows that the MSE of both methods decreases linearly as the input SNR increases. This result confirms the analysis results in (2.13) and (2.16). It is clearly observed that the LS-2SCE method outperforms the Conv-CE method because more bits can be used for channel estimation in the former method.

To investigate the performance of the proposed LS-2SCE method in a fading environment, a two-path (with equal average power) Rayleigh fading channel is simulated with the first path located at the 1st sample and the second path randomly located from the 2nd to the  $L$ th sample. The average SNR is varied from 10 to 20 dB again. Note that the complex gains of the two fading paths were generated independently using Jake's fading channel model [51], at a vehicle speed of 60 km/h, and at a carrier frequency of 900 MHz. Fig. 2.8 plots the simulation results. The MSE performances in Fig. 2.8 are worse than the corresponding MSE performances in Fig. 2.7. This is because the fading phenomenon affects the accuracy of the channel estimation. Nevertheless, the improvement in the MSE ratio of the Conv-CE method to the LS-2SCE method is not greatly reduced. From Fig. 2.8, it is clearly observed that the LS-2SCE method still outperforms the Conv-CE method even in a fading environment.

To examine the fading effects, the two-path fading channel model above is used again; the vehicle speed was varied from 3 km/h (slow fading) to 300 km/h (fast fading), and the input SNR was fixed at 15 dB. The corresponding results are shown in Fig. 2.9. It is clearly observed that the MSE of the Conv-CE method is larger than the MSE of the proposed LS-2SCE method at different vehicle speeds. These results further demonstrate that the LS-2SCE method outperforms the Conv-CE method in both slow and fast fading channels.

## 2.6 Conclusion

In this chapter, a novel channel estimation method is proposed in order to fully utilize the known data in the guard interval for channel estimation. The proposed method was designed as a two-stage procedure. In the first stage, the LS algorithm was used to compute the initial CIR estimation based on the normal training sequence. Based

on the initial CIR estimation, the maximum channel memory can be estimated. In the second stage, the estimated maximum channel memory was used to extract the uncorrupted data in the guard interval. Finally, both the uncorrupted data and the normal training sequence were sent to the LS algorithm again to estimate a fine-tuned CIR. Both a theoretical analysis and computer simulations were carried out to confirm that the proposed LS-2SCE method outperforms the Conv-CE method. Overall, we demonstrated that the LS-2SCE is an efficient and feasible method.



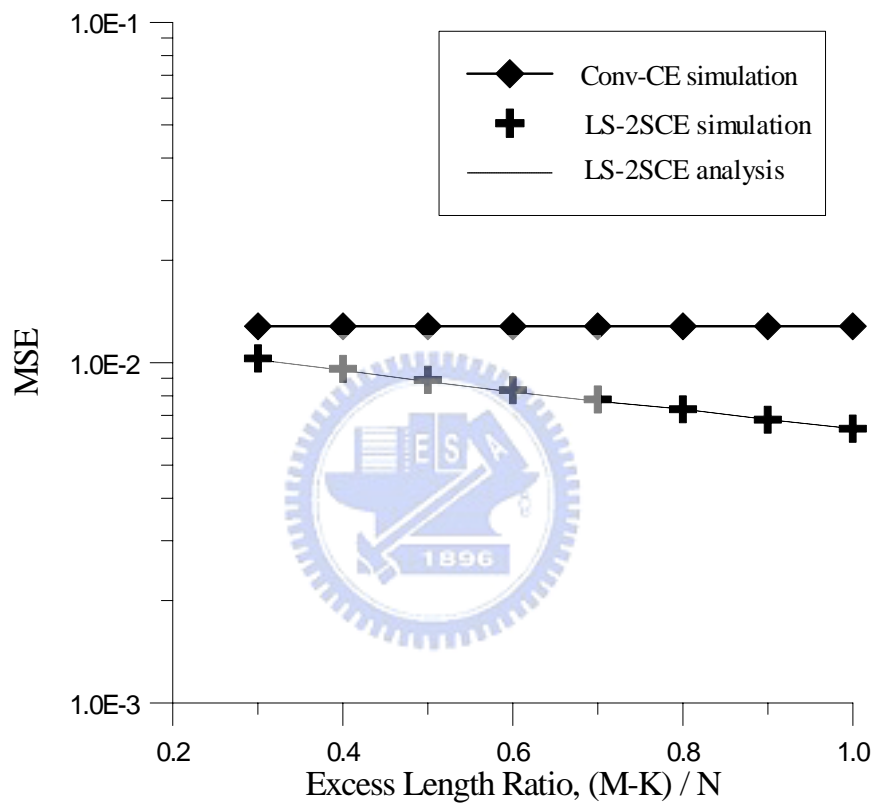


Fig. 2.3: MSE versus excess length ratio in an equal-gain two-path fixed channel at an SNR of 15 dB.

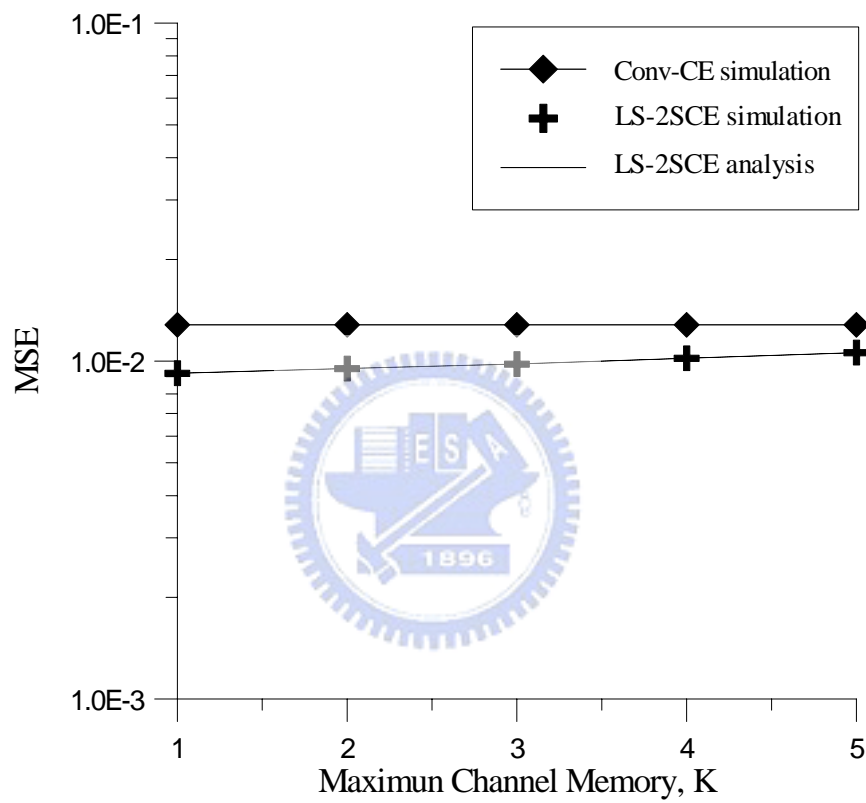


Fig. 2.4: MSE versus different maximum channel memory  $K$  in an equal-gain two-path channel at an SNR of 15 dB.

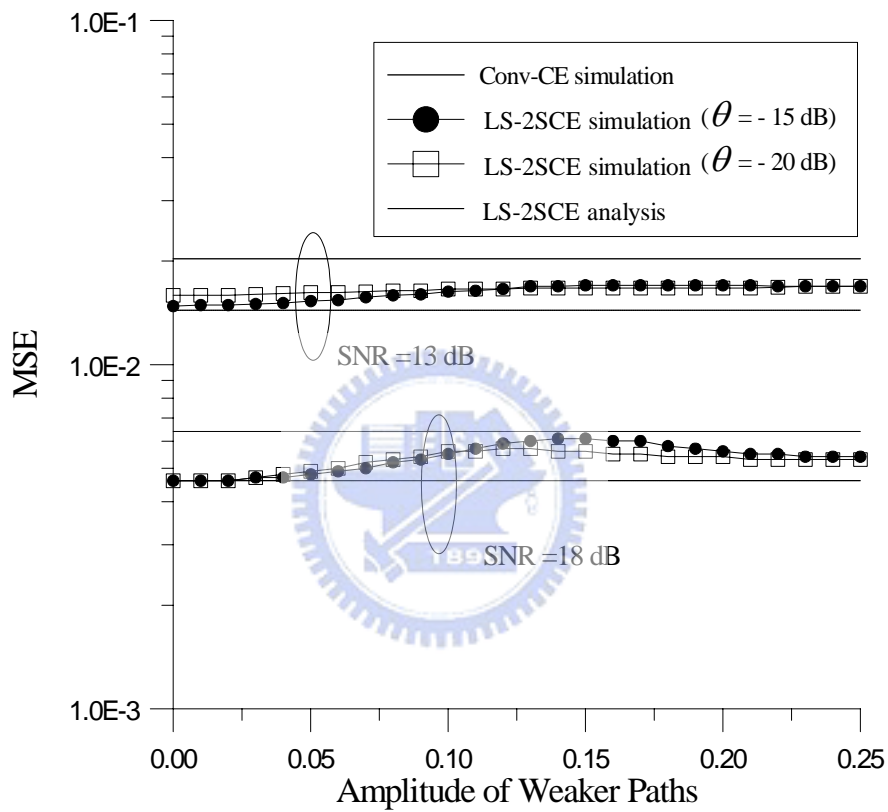


Fig. 2.5: MSE versus amplitude of the weaker paths in a multipath channel. This channel has two strong paths of equal power followed by four weaker paths also of equal power.

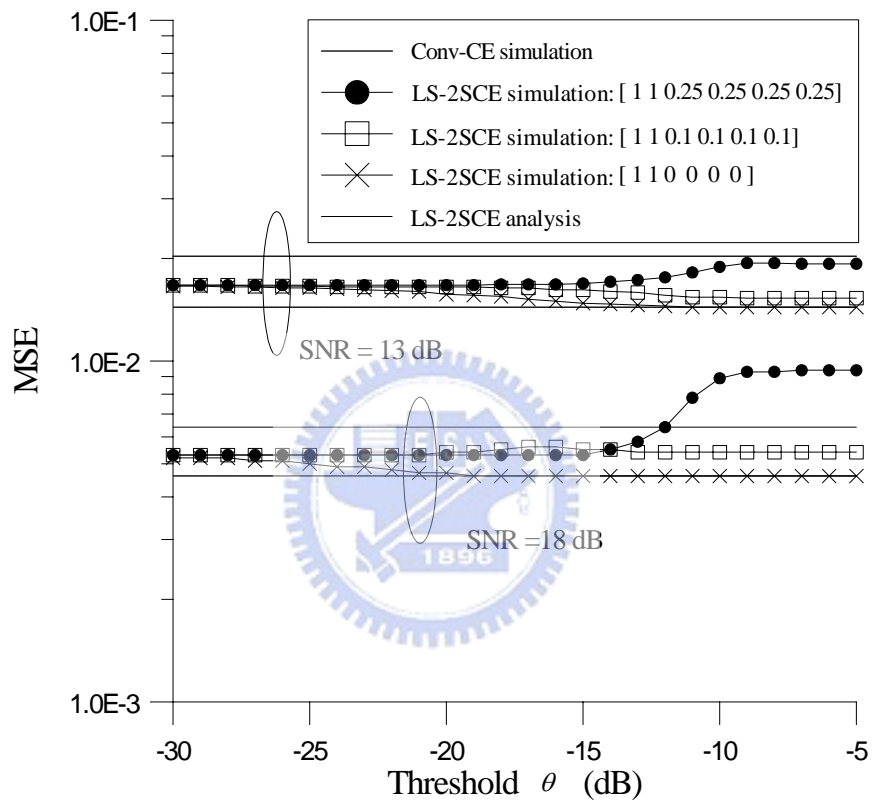


Fig. 2.6: MSE versus threshold  $\theta$  in three different multipath channels with the same channel model as described in Fig. 2.5.

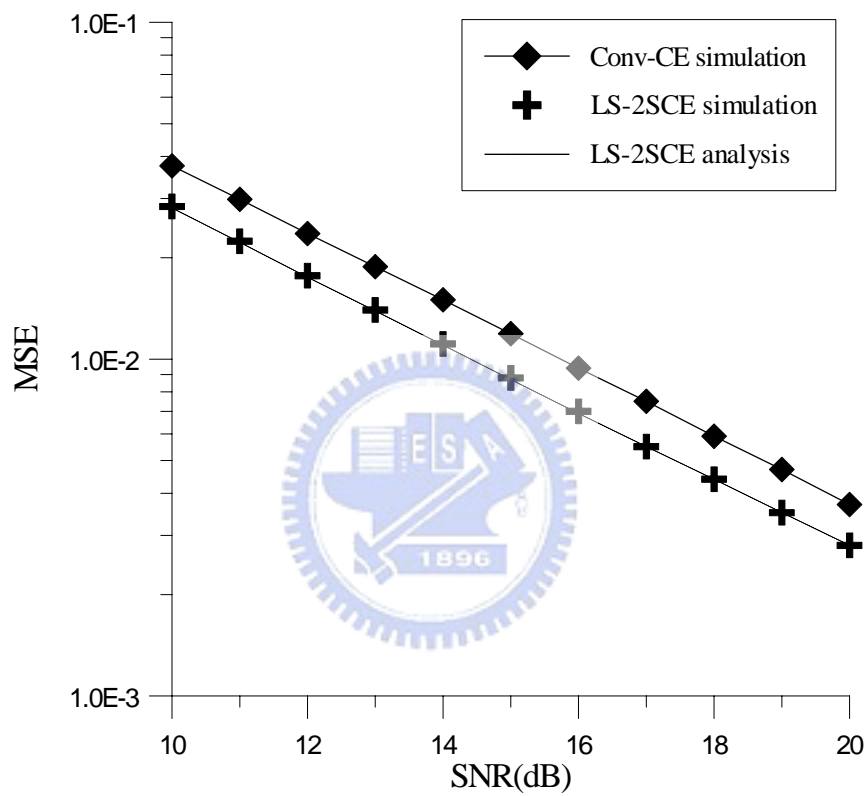


Fig. 2.7: MSE versus SNR in an equal-gain two-path fixed channel with the first path located at the 1st sample and the second path randomly located from the 2nd to the  $L$ th sample.

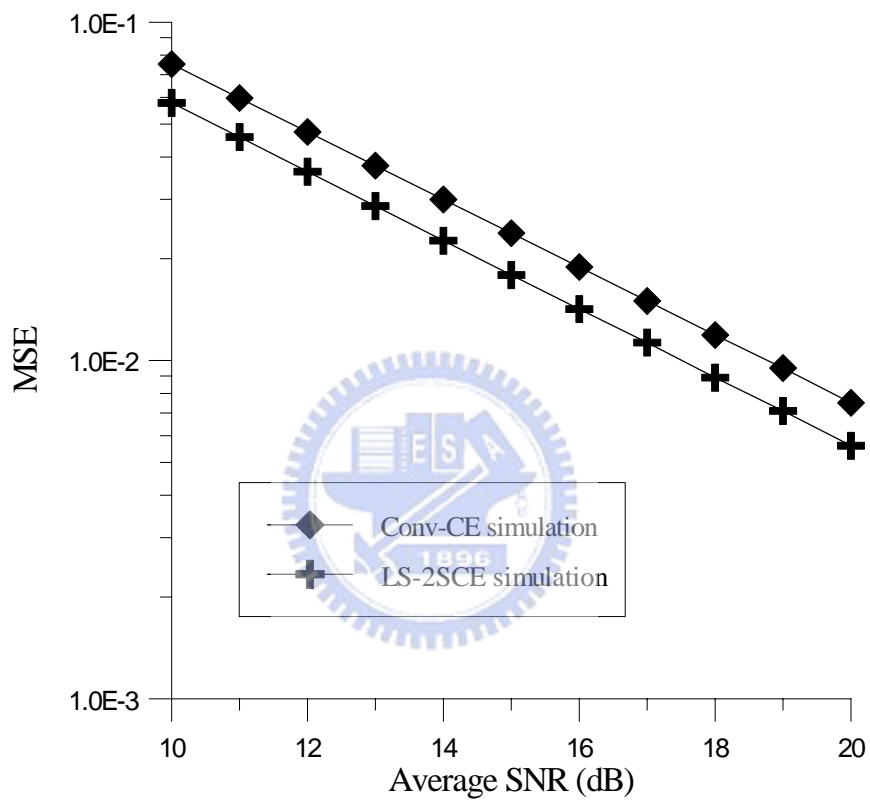


Fig. 2.8: MSE versus average SNR in a two-path Rayleigh fading channel with the first path located at the first sample and the second path randomly located from the second to the sixth sample at the vehicle speed of 60 km/h.

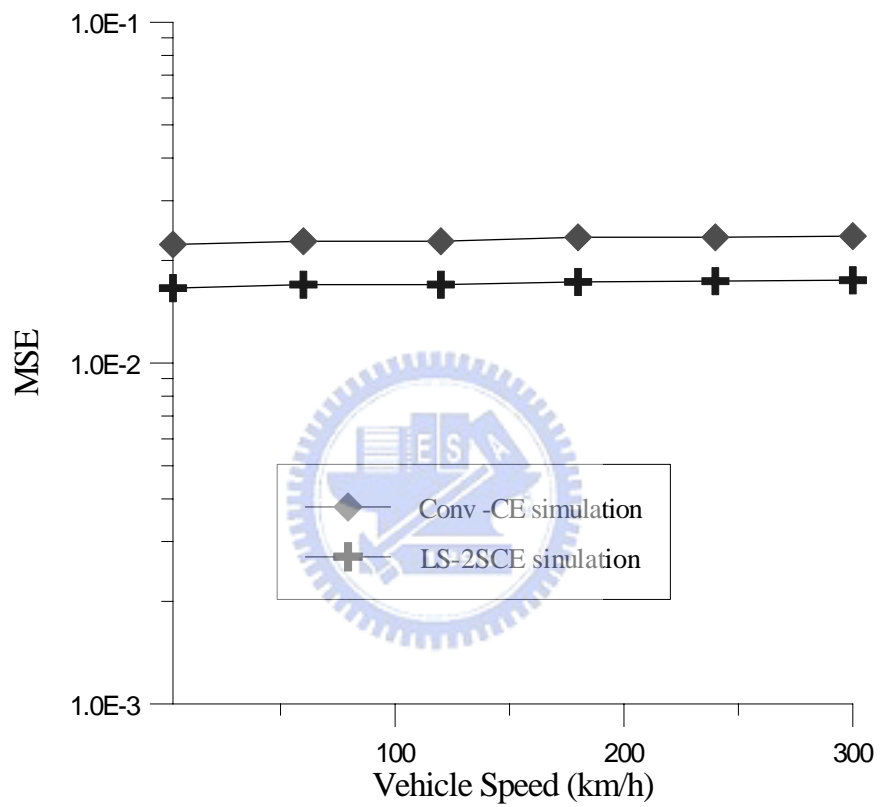


Fig. 2.9: MSE versus different vehicle speeds in a two-path Rayleigh fading channel with the same channel model as described in Fig. 2.8 at an SNR of 15 dB.

# Chapter 3

## A Multipath Interference Cancellation Based Two-stage Channel Estimation Method

### 3.1 Introduction

Since the length of the guard interval is usually larger than the length of the effective multipath delay in a typical mobile radio communication environment, we proposed the LS-2SCE method in Chapter 2 to fully utilize the uncorrupted data in the guard interval to improve the performance of channel estimation. Also, we verified the benefits of the LS-2SCE method.

However, the LS-2SCE method needs to execute the LS algorithm on an augmented matrix in the second stage, the computation complexity is high. To avoid this computation complexity, a multipath interference cancellation [36]–[38] based two-stage channel estimation (MIC-2SCE) method is proposed in this chapter. In the first stage, a conventional channel estimation method was used to estimate the CIR based on the normal training sequence. In order to determine the maximum channel memory and the effective paths, we discarded those weaker paths whose amplitude (normalized by the peak amplitude) smaller than a certain threshold  $\theta$ . The threshold  $\theta$  was defined as a small factor of the peak amplitude of all estimated paths. Then the maximum channel memory and the effective paths were estimated. In the second stage, both the maximum channel memory and the effective paths were used to locate

the uncorrupted data in the received training sequence and to reconstruct the individual path data of each effective path in this uncorrupted region. Note that the ISI in this region was generated by the known training sequence only. Therefore, the individual path interference could be calculated and the individual path signal could be extracted. Since there was only a single path data remained in each individual path signal, the correlation method could be used to estimate each individual path gain. Then, the individual path signal was used to correlate with the corresponding data in the training sequence to obtain the fine-tuned CIR. Since extra bits were utilized for channel estimation, the proposed method led to an improved performance compared to conventional methods. In addition, only the multipath interference cancellation and the correlative channel estimation were added, the computation complexity was relatively low. To verify the efficiency of the proposed method, both theoretical analysis and computer simulations were done. Computer simulation results confirm the analytical results and demonstrate that the proposed method really outperforms a conventional single-stage channel estimation method.

This chapter describes the operation principles, conducts theoretical analysis and evaluates the performance of the proposed method. In Section 3.2, the conventional channel estimation methods are described. In Section 3.3, the details of the proposed method including the function of each stage and the algorithms used are presented. In Section 3.4, theoretical analysis on the proposed method is given. Computer simulation results are presented in Section 3.5. Finally, discussion and conclusion are given in Section 3.6.

## 3.2 The Conventional Channel Estimation Methods

A conventional channel estimation method is usually based on a known training sequence [8]. A guard interval is typically generated from the cyclic extension of the normal training sequence [42], [43]. Let a binary normal training sequence be denoted as  $\{s_0, s_1, \dots, s_{N-1}\}$ , where  $s_i \in \{1, -1\}$ . Including a cyclically extended prefix, the transmitted training sequence is then given by  $\{s_{N-M}, s_{N-M+1}, \dots, s_{(N-1)}, s_0, s_1, \dots, s_{N-1}\}$ , where  $M$  is the length of the guard interval and  $M \geq L-1$ . The training sequence including its related parameters is depicted in Fig. 3.1. Note that the training sequence can be divided into the  $N$ -bit normal training sequence portion and the  $M$ -bit prefix

portion (guard interval).

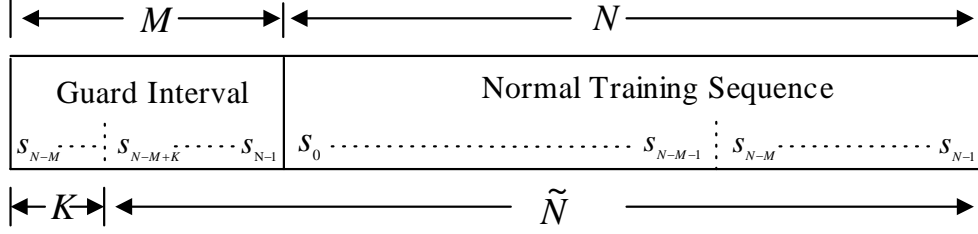


Fig. 3.1: The guard interval and the normal training sequence of the training sequence.

$K$  and  $\tilde{N}$  denote the maximum channel memory and the extended normal training sequence, respectively.

Considering a digital data communication system in a multipath channel with a maximum delay spread of  $L$  samples, the received signal associated with the normal training sequence can be expressed in an  $N \times 1$  vector  $\mathbf{r}$  as given by

$$\mathbf{r} = \mathbf{S}\mathbf{h} + \mathbf{n} \quad (3.1)$$

where the complex CIR vector  $\mathbf{h} = [h_0 \ h_1 \ \dots \ h_{L-1}]^T$  with  $T$  denoting the transpose operator, and the  $N \times 1$  vector  $\mathbf{n}$  denotes the additive white Gaussian noise (AWGN) samples with zero mean and variance  $\sigma_n^2$ . The  $N \times L$  normal training sequence matrix  $\mathbf{S}$  is then given by (2.3) (in Section 2.2)

Based on executing a LS algorithm on the normal training sequence, the optimum result of estimated CIR is [44]

$$\hat{\mathbf{h}}_{ls} = (\mathbf{S}^H \mathbf{S})^{-1} \mathbf{S}^H \mathbf{r} \quad (3.2)$$

where  $(\cdot)^{-1}$  and  $H$  denote the matrix inverse operator and the Hermitian operator, respectively. The above LS channel estimation solution has been shown to be the best linear unbiased estimate of the CIR [45]. A normal training sequence is said to be perfect if its associated correlation matrix  $\mathbf{S}^H \mathbf{S}$  is diagonal allowing for the mean squared channel estimation error to be minimized [46]. In this case, the solution in (3.2) can be further simplified to

$$\hat{\mathbf{h}}_{ls} = \frac{1}{N} \mathbf{S}^H \mathbf{r} \quad (3.3)$$

where  $N$  is the length of the normal training sequence. The simplified channel estimator can be obtained by correlating the normal training sequence with its associated received signal. In this case, the LS channel estimation method is the same as the correlative channel estimation method. Hereafter, this chapter uses the term Conv-CE method to denote the conventional LS channel estimation method based on the normal training sequence for simplicity and consistency.

### 3.3 The Proposed MIC-2SCE Method

The details of the proposed method, as shown in Fig. 3.2, are described below:

#### 3.3.1 The first stage

The purpose of the first stage is to estimate the effective paths and the maximum channel memory. An initial estimation of CIR can be obtained by executing the Conv-CE method. In particular, if the correlation matrix  $\mathbf{S}^H \mathbf{S}$  is diagonal, meaning that the correlations among different paths are zero, the Conv-CE method can be reduced to the correlative channel estimation method.

After obtaining the initial CIR estimation, the strongest path among all the estimated paths is selected as the reference path and its amplitude is denoted as  $A_{\max}$ . To select the effective paths, all the paths whose amplitude (normalized by  $A_{\max}$ ) is smaller than a threshold  $\theta$  are set to zero and then the remaining nonzero paths are referred to as effective paths. Note that the threshold  $\theta$  is a system parameter which is related to the peak amplitude  $A_{\max}$ .

Accordingly, the last effective path can be found and its position is located. If the position of the first path is set to 0, the maximum channel memory  $K$ , is set to the position of the last effective path. Currently, all the effective paths are collected to form an  $L \times 1$  CIR vector  $\hat{\mathbf{h}}$ , and the elements of this vector are either the effective path gains or zeros.

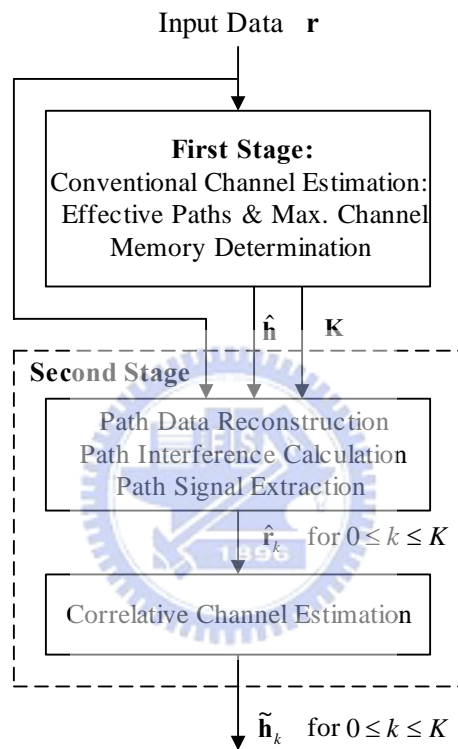


Fig. 3.2: A flow chart of the proposed MIC-2SCE method

### 3.3.2 The second stage

After the maximum channel memory  $K$  is obtained in the first stage, it can be used to locate the  $M - K$  uncorrupted data in the guard interval. By combining the  $M - K$  uncorrupted data with the normal training sequence, we can obtain an extended normal training sequence with length  $\tilde{N} = M - K + N$  shown in Fig. 3.1. Under the condition that the threshold  $\theta$  used in the first stage is set small enough, the discarded paths are relatively weak and the ISI effect caused by the adjacent random data can be neglected. Then the received signal vector  $\tilde{\mathbf{r}}$  associated with the extended normal training sequence can be approximately written as

$$\tilde{\mathbf{r}} \approx \tilde{\mathbf{S}}\mathbf{h} + \tilde{\mathbf{n}} \quad (3.4)$$

where the  $\tilde{N} \times 1$  vector  $\tilde{\mathbf{n}}$  denotes the extended noise vector, and the  $\tilde{N} \times L$  augmentation matrix  $\tilde{\mathbf{S}}$  is composed of the training sequence and can be expressed as below

$$\tilde{\mathbf{S}} = \begin{bmatrix} s_{N-M+K} & s_{N-M+K-1} & \cdots & s_{N-M+K-L+1} \\ s_{N-M+K+1} & s_{N-M+K} & \cdots & s_{N-M+K-L+2} \\ \vdots & \vdots & \ddots & \vdots \\ s_{N-1} & s_{N-2} & \cdots & s_{N-L} \\ s_0 & s_{N-1} & \cdots & s_{N-L+1} \\ s_1 & s_0 & \cdots & s_{N-L+2} \\ \vdots & \vdots & \ddots & \vdots \\ s_{N-1} & s_{N-2} & \cdots & s_{N-L} \end{bmatrix} = [\tilde{\mathbf{s}}_0 \quad \tilde{\mathbf{s}}_1 \quad \cdots \quad \tilde{\mathbf{s}}_{L-1}] \quad (3.5)$$

Note that the vector  $\tilde{\mathbf{s}}_k$  for  $k = 0, 1, \dots, L-1$  denote the  $k$ th column vector of matrix  $\tilde{\mathbf{S}}$ .

Typically, the normal training sequence is designed to have ideal correlation property, i.e., its associated correlation matrix  $\mathbf{S}^H\mathbf{S}$  is diagonal. However, the extended normal training sequence usually does not preserve this property and it will generate ISI due to multipath propagation [52], [53]. In order to use the correlation method in the second stage, we must remove the ISI and extract each individual path signal from the received signal.

From (3.4) and (3.5), we know that the ISI in the received signal vector  $\tilde{\mathbf{r}}$  is caused by solely the known training sequence. Therefore, the  $k$  th effective path data can be reconstructed by multiplying the  $k$  th column vector  $\tilde{\mathbf{s}}_k$  by the  $k$  th effective path gain (i.e.,  $\tilde{\mathbf{s}}_k h_k$ ).

Let us define an  $L \times L$  diagonal matrix  $\mathbf{D}_k$  as a selection matrix in which the  $k$  th diagonal entry is zero and the others are one. Then the  $k$  th path interference for the  $k$  th effective path can be calculated by the matrix operation  $\tilde{\mathbf{S}}\mathbf{D}_k\hat{\mathbf{h}}$ . Accordingly, the  $\tilde{N} \times 1$  signal vector of individual path  $\tilde{\mathbf{r}}_k$  for  $0 \leq k \leq K$  can be extracted from the received signal by

$$\tilde{\mathbf{r}}_k = \tilde{\mathbf{r}} - \tilde{\mathbf{S}}\mathbf{D}_k\hat{\mathbf{h}} \quad (3.6)$$

In the ideal situation, the estimated CIR  $\hat{\mathbf{h}} = \mathbf{h}$ , then (3.6) will be reduced to  $\tilde{\mathbf{r}}_k = \tilde{\mathbf{s}}_k h_k + \tilde{\mathbf{n}}$ . Since most of the multipath interference can be successfully cancelled, the  $k$  th path gain  $\tilde{h}_k$  for  $0 \leq k \leq K$  can be estimated by the following correlation operation:

$$\tilde{h}_k = \tilde{\mathbf{s}}_k^H \tilde{\mathbf{r}}_k / \tilde{N} \quad (3.7)$$

Therefore, an  $L \times 1$  vector  $\tilde{\mathbf{h}}$  of a fine-tuned CIR can be obtained by collecting all the estimated path gains.

The algorithm of the MIC-2SCE method is summarized as follows:

### Stage I.

1. Set the system parameters: the maximum CIR length  $L$  and the threshold  $\theta$ .
2. Obtain an initially estimated CIR  $\hat{\mathbf{h}}_{ls}$ , according to (3.2).
3. Find the strongest path:  $A_{\max} = \max | \hat{h}_{ls}(i) |$ , where  $\hat{h}_{ls}(i)$  for  $i = 0, 1, \dots, L-1$  denote the  $i$  th entry of the vector  $\hat{\mathbf{h}}_{ls}$ .

4. Set the weak paths to zero: If  $\left(\left|\hat{h}_{i_s}(i)\right|/A_{\max}\right) < \theta$ , then let  $\hat{h}_{i_s}(i) = 0$  for  $i = 0, 1, \dots, L-1$ .
5. Determine the maximum channel memory  $K$ : Find the last nonzero path  $\hat{h}_{i_s}(i)$ . Then, set the maximum channel memory  $K = i$ .
6. Collect all the nonzero paths to form an effective path vector,  $\hat{\mathbf{h}}$ .

### Stage II.

1. Locate the uncorrupted data and form the augmentation matrix  $\tilde{\mathbf{S}}$ .
2. Extract the individual path signal vector  $\tilde{\mathbf{r}}_k$  for  $0 \leq k \leq K$ , according to (3.6).
3. Obtain the  $k$ th path gain  $\tilde{h}_k$  for  $0 \leq k \leq K$ , according to (3.7).
4. Collect all the path gains to form a fine-tuned estimated CIR  $\tilde{\mathbf{h}}$ .

## 3.4 Performance Analysis

In this section, theoretical analysis is given to verify that the performance of the proposed method is superior to the Conv-CE method.

For brevity, the following analysis of the MIC-2SCE method is based on the assumption that the paths discarded in the first stage are very weak. When the effect of the discarded paths are relatively small compared to the noise, it can be neglected and the equality in (3.4) holds. According to the LS solution in (3.2), the corresponding mean square error (MSE) of the conventional LS channel estimator is given by [44]

$$MSE_{conv} = \sigma_n^2 \text{tr}\left\{\left(\mathbf{S}^H \mathbf{S}\right)^{-1}\right\} \quad (3.8)$$

where  $\text{tr}(\cdot)$  denotes the trace operator. In the case of a perfect normal training sequence, its associated correlation matrix  $\mathbf{S}^H \mathbf{S}$  is diagonal. The minimum MSE can be achieved and the LS channel estimation method can be simplified to the correlative channel estimation method. When there are  $P$  effective paths, the MSE of the

Conv-CE method in (3.8) can be simply written as

$$\text{MSE}_{conv} = \sigma_n^2 \times P / N \quad (3.9)$$

Substituting (3.1) into (3.2) and neglecting the weak paths, we can derive the following relationship:

$$\hat{\mathbf{h}}_{1s} = \mathbf{h} + (\mathbf{S}^H \mathbf{S})^{-1} \mathbf{S}^H \mathbf{n} \approx \hat{\mathbf{h}} \quad (3.10)$$

Note that the  $(\mathbf{S}^H \mathbf{S})^{-1} \mathbf{S}^H \mathbf{n}$  term dominates the estimation error in the LS method. Substituting (3.6) into (3.7), the estimated  $k$  th path gain can be rewritten as

$$\begin{aligned} \tilde{h}_k &= \tilde{\mathbf{s}}_k^H (\tilde{\mathbf{r}} - \tilde{\mathbf{S}} \mathbf{D}_k \hat{\mathbf{h}}) / \tilde{N} \\ &= \tilde{\mathbf{s}}_k^H (\tilde{\mathbf{S}} \mathbf{h} + \tilde{\mathbf{n}} - \tilde{\mathbf{S}} \mathbf{D}_k \hat{\mathbf{h}}) / \tilde{N} \\ &= \tilde{\mathbf{s}}_k^H \left\{ \tilde{\mathbf{S}} \mathbf{h} + \tilde{\mathbf{n}} - \tilde{\mathbf{S}} \mathbf{D}_k [\mathbf{h} + (\mathbf{S}^H \mathbf{S})^{-1} \mathbf{S}^H \mathbf{n}] \right\} / \tilde{N} \\ &= h_k + \tilde{\mathbf{s}}_k^H [\tilde{\mathbf{n}} - \tilde{\mathbf{S}} \mathbf{D}_k (\mathbf{S}^H \mathbf{S})^{-1} \mathbf{S}^H \mathbf{n}] / \tilde{N} \end{aligned} \quad (3.11)$$

Taking the expectation of the difference between the estimated path gain  $\tilde{h}_k$  and true path gain  $h_k$ , and after some detailed linear algebraic operations, we are able to arrive at the MSE associated with the  $k$ th path

$$\begin{aligned} \text{MSE}_k &= E \left\{ \left| \tilde{\mathbf{s}}_k^H [\tilde{\mathbf{n}} - \tilde{\mathbf{S}} \mathbf{D}_k (\mathbf{S}^H \mathbf{S})^{-1} \mathbf{S}^H \mathbf{n}] / \tilde{N} \right|^2 \right\} \\ &= \sigma_n^2 / \tilde{N}^2 \times \left\{ \tilde{N} + \tilde{\mathbf{s}}_k^H \tilde{\mathbf{S}} \mathbf{D}_k (\mathbf{S}^H \mathbf{S})^{-1} \mathbf{D}_k \tilde{\mathbf{S}}^H \tilde{\mathbf{s}}_k \right\} \end{aligned} \quad (3.12)$$

where  $E\{\cdot\}$  and  $|\cdot|$  denote the expectation operator and the absolute operator, respectively. A more detailed derivation is described in Appendix. Under the condition that the correlations among different time shifts of the original training sequence are small, i.e.,  $\tilde{\mathbf{s}}_i^H \tilde{\mathbf{s}}_j / \tilde{N} \ll 1$  for  $i \neq j$ , we have

$$\tilde{\mathbf{s}}_k^H \tilde{\mathbf{S}} \mathbf{D}_k (\mathbf{S}^H \mathbf{S})^{-1} \mathbf{D}_k \tilde{\mathbf{S}}^H \tilde{\mathbf{s}}_k \ll \tilde{N} \quad (3.13)$$

such that (3.12) can be reduced to

$$\text{MSE}_k \approx \sigma_n^2 / \tilde{N} \quad (3.14)$$

In the case of  $P$  effective paths, the MSE of the proposed method can be expressed as

$$\text{MSE}_{\text{MIC2S}} \approx \sigma_n^2 \times P / \tilde{N} \quad (3.15)$$

According to (3.9) and (3.15), we know that the MSE performance of the MIC-2SCE method is approximately  $\tilde{N}/N$  times better than that of the Conv-CE method. In the case of  $\tilde{N} = N$ , there is no uncorrupted data in the guard interval, and the result of  $\text{MSE}_{\text{MIC2S}} = \text{MSE}_{\text{conv}}$  can be obtained from (3.9) and (3.15). In the case of  $\tilde{N} = 2N$ , there are  $N$  bits of uncorrupted data in the guard interval, and the result of  $\text{MSE}_{\text{MIC2S}} = \frac{1}{2} \text{MSE}_{\text{conv}}$  can also be obtained from (3.9) and (3.15).

### 3.5 Computer Simulations

To evaluate the performance of the proposed MIC-2SCE method, a series of computer simulations were carried out under different channel conditions. In order to compare the performance of different channel estimators, the MSE between the ideal effective path vector,  $\mathbf{h}_{\text{eff}}$ , and the estimated effective path vector,  $\tilde{\mathbf{h}}$ , was defined as

$$\text{MSE} = E \left\{ \left\| \mathbf{h}_{\text{eff}} - \tilde{\mathbf{h}} \right\|^2 \right\} / E \left\{ \left\| \mathbf{h} \right\|^2 \right\} \quad (3.16)$$

where  $\|\bullet\|$  denotes the 2-norm operator.

Our simulations were divided into two parts. In the first part, the general behavior of the MIC-2SCE method was investigated in a multipath environment. In the second part, the data burst of GSM was employed to examine the performance of the MIC-2SCE method in both a two-path fixed channel and a two-path fading channel. For comparison purpose, the corresponding results of the Conv-CE method were also included.

In all our simulations, the power of the CIR vector was normalized to one. The maximum CIR length  $L$  was set to 6 and the binary phase shift keying (BPSK) modulation method was assumed.

### 3.5.1 General Behavior of the Proposed Channel Estimator

In the first part of our simulations, the input SNR was set to 10 dB and the central 16-bit pattern of a GSM midamble which was defined by ETSI (European Telecommunications Standards Institute) was used as the normal training sequence [25]. The threshold  $\theta$  used in the first stage was set to  $-10$  dB relative to the peak amplitude of all the estimated paths, and the analytical result of the MIC-2SCE method calculated from (3.15) was plotted as the dashed line in each figure.

To investigate the effect of the guard interval length on channel estimation in an equal-gain two-path fixed channel, the first path was set at the 1st sample, the second path was set at the 2nd sample, and the guard interval length varied from 7 to 17. The corresponding MSE versus the ratio of the length of the extended normal training sequence to the length of the normal training sequence is shown in Fig. 3.3. This ratio,  $\tilde{N}/N$ , is referred to as the useful length ratio. It is observed that the MSE of the simulated MIC-2SCE method is close to the analytical result and it decreases as the useful length ratio increases. This is because the length of the uncorrupted data is directly related to the guard interval length. On the contrary, the MSE of the Conv-CE method is approximately a constant due to the fixed length of the normal training sequence. For example, when the useful length ratio is 2, the MSE of the proposed method is reduced to one-half (50%) of that of the Conv-CE method.

To evaluate the effect of the maximum channel memory on the performance of the MIC-2SCE method, the guard interval length was set to 10, and an equal-gain two-path channel was modeled in such a way that the first path was at the 1st sample and the second path was changed from the 2nd to the  $L$ th sample. The corresponding MSE versus the variation in maximum channel memory is shown in Fig. 3.4. It is observed that the MSE of the MIC-2SCE method is close to the analytical result and increases as the maximum channel memory increases. This is because fewer bits are used for channel estimation in the MIC-2SCE method as the maximum channel memory increases.

To examine the effect of weaker paths on the performance of the MIC-2SCE method, the guard interval length was again set to 10, and a channel with two strong paths of equal power followed by two weaker paths also of equal power was

employed in this simulation. The amplitudes of strong paths were set to 1 and the amplitudes of weaker paths varied from 0 to 0.1. The corresponding MSE versus different amplitudes of the weaker paths is shown in Fig. 3.5. Note that the amplitude levels as shown in Fig. 3.5 and as mentioned above are not normalized. It is observed that the analytical results are consistent with the simulation results when the amplitudes are small. However, the MSEs for both curves slightly increase as the amplitudes increase. This is because the total effect of the discarded paths becomes more significant and can lead to performance degradation in MSE. Nevertheless, the ratio of the MSE of the Conv-CE method to the MSE of the MIC-2SCE method remains approximately constant.

### 3.5.2 Performance Enhancement with the Proposed Channel Estimator

In the second part of our simulations, the GSM burst structure was employed, and the BPSK modulation method was simulated at a data rate of 270.833 kbits/sec. When the GSM midamble was mapped into the structure of Fig. 3.1, it could be separated into a 10-bit guard interval and a 16-bit normal training sequence. In addition to the two channel estimation methods discussed above, both the LS-2SCE method [54] and the correlative two-stage channel estimation (Corr-2SCE) method were also included for comparison. Note that the Corr-2SCE method directly executes a correlative channel estimation on the received signal associated with the extended training sequence, i.e., it does not execute the MIC algorithm in the second stage.

To illustrate the performance of the MIC-2SCE method in an equal-gain two-path fixed channel, the first path was located at the 1st sample and the second path was set at the 2nd sample. The threshold  $\theta$  was set to  $-10$  dB and the average SNR varied from 5 to 15 dB. The corresponding results are shown in Fig. 3.6. This figure shows that the MSEs of both the MIC-2SCE and LS-2SCE methods are close to the analytical result which is calculated from (3.15). This figure also shows that except for the Corr-2SCE method, the MSEs of all other methods decrease linearly as the input SNR increases. This result confirms the analytical results of (3.9) and (3.15). Although the Corr-2SCE method performs better than the Conv-CE method in the low SNR region, it is inferior to the Conv-CE method in the high SNR region. This is

because the noise effect dominates the accuracy of channel estimation when the SNR is low. However, as the SNR increases, the ISI effect caused by the nonideal correlation property of the extended normal training sequence becomes significant and can lead to performance degradation in MSE. From Fig. 3.6, it is clearly observed that the proposed method performs as well as the LS-2SCE method and outperforms the other two methods.

To investigate the performance of the proposed method in a fading environment, a two-path (with equal average power) Rayleigh fading channel was simulated with the first path located at the 1st sample and the second path at the 2nd sample. The threshold  $\theta$  was set to  $-15$  dB and the average SNR varied from 5 to 15 dB again. Note that the complex gains of the two fading paths were generated independently using Jake's fading channel model [51], at a vehicle speed of 60 km/h, and at a carrier frequency of 900 MHz. Fig. 3.7 plots the simulation results. The MSE performance in Fig. 3.7 is worse than the corresponding MSE performance in Fig. 3.6. This is because the fading phenomenon affects the accuracy of the channel estimation. Nevertheless, the general trend in the MSE performance of these four channel estimation methods remains the same. It is clearly observed that the proposed method still performs approximately the same as the LS-2SCE method and outperforms the other two methods even in a fading environment.

To examine the fading effects, the two-path fading channel model above was used again; the vehicle speed varied from 3 km/h (slow fading) to 300 km/h (fast fading), and the average SNR was fixed at 10 dB. The threshold  $\theta$  was set to  $-15$  dB and the corresponding results are shown in Fig. 3.8. It is clearly observed that the MSE of the proposed method is almost identical to that of the LS-2SCE method, and these two MSEs are also smaller than the MSEs of the other two methods at different vehicle speeds.

### 3.6 Discussion and Conclusion

As far as the computation complexity of the channel estimation methods mentioned above, the Conv\_CE method is the lowest because it only has a single stage. Since the other three two-stage methods have the same computation complexity in the first stage, we only compare their efforts in computation (in number of multiplications) in

the second stage. By replacing  $\mathbf{S}$  with  $\tilde{\mathbf{S}}$  and  $\mathbf{r}$  with  $\tilde{\mathbf{r}}$  in (3.2), the computation complexity [55] of the LS-2SCE method is  $(L^2 \times \tilde{N} + L^3 + L^2 \times \tilde{N} + L \times \tilde{N})$ . As a comparison, the proposed MIC-2SCE method needs to execute the multipath interference cancellation and to perform the correlative channel estimation, and they need  $(L \times (L-1) \times \tilde{N})$  and  $(L \times \tilde{N})$  multiplications, respectively. Finally, the Corr-2SCE method needs only to execute the correlative channel estimation according to (3.7) with  $(L \times \tilde{N})$  multiplications. In summary, the approximate computation complexity of the three two-stage methods are listed as below:

- LS-2SCE:  $(L^2 \times \tilde{N} + L^3 + L^2 \times \tilde{N} + L \times \tilde{N})$
- MIC-2SCE:  $(L \times (L-1) \times \tilde{N} + L \times \tilde{N})$
- Corr-2SCE:  $(L \times \tilde{N})$

In this chapter, a novel MIC-2SCE method with a relatively low computation complexity is proposed to fully utilize the uncorrupted data in the guard interval of a training sequence for channel estimation. Jointly using the knowledge of maximum channel memory and effective paths which have been estimated in the first stage, the individual path interference could be reconstructed and the individual path signal could be extracted in the uncorrupted region. Since the multipath interference was removed in the individual path signal, we could use the correlation method operating on an extended normal training sequence to estimate a fine-tuned CIR in the second stage. Both theoretical analysis and computer simulations confirm that the proposed method outperforms the Conv-CE method. Furthermore, from our simulation results and discussion on computation complexity, we conclude that the MSE performance of the MIC-2SCE method is approximately equal to that of the LS-2SCE method, but the former method has a lower computation complexity. Therefore, the proposed MIC-2SCE method is a feasible and useful channel estimation scheme.

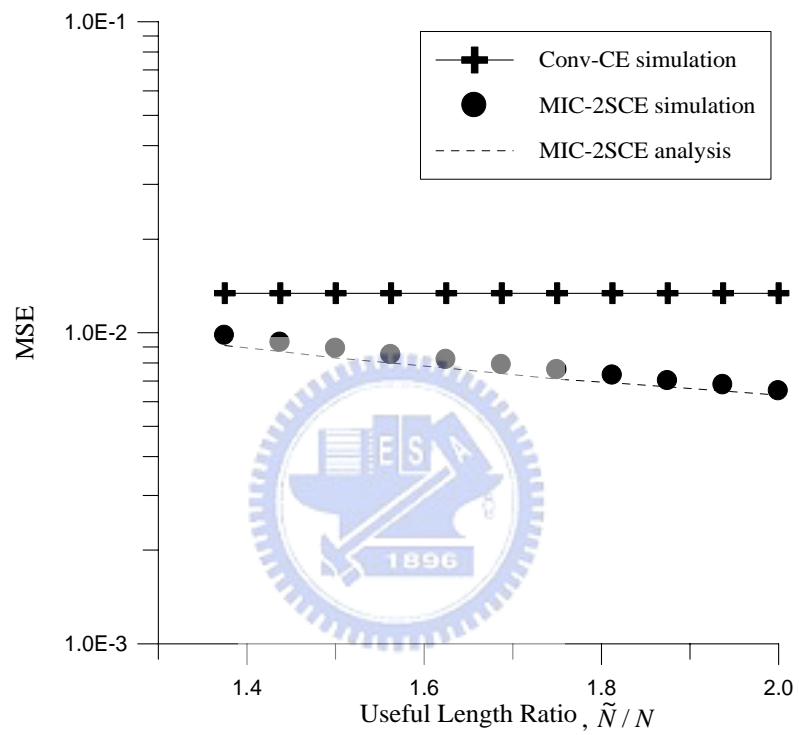


Fig. 3.3: MSE versus useful length ratio,  $\tilde{N}/N$ , in an equal-gain two-path fixed channel at an SNR of 10 dB.

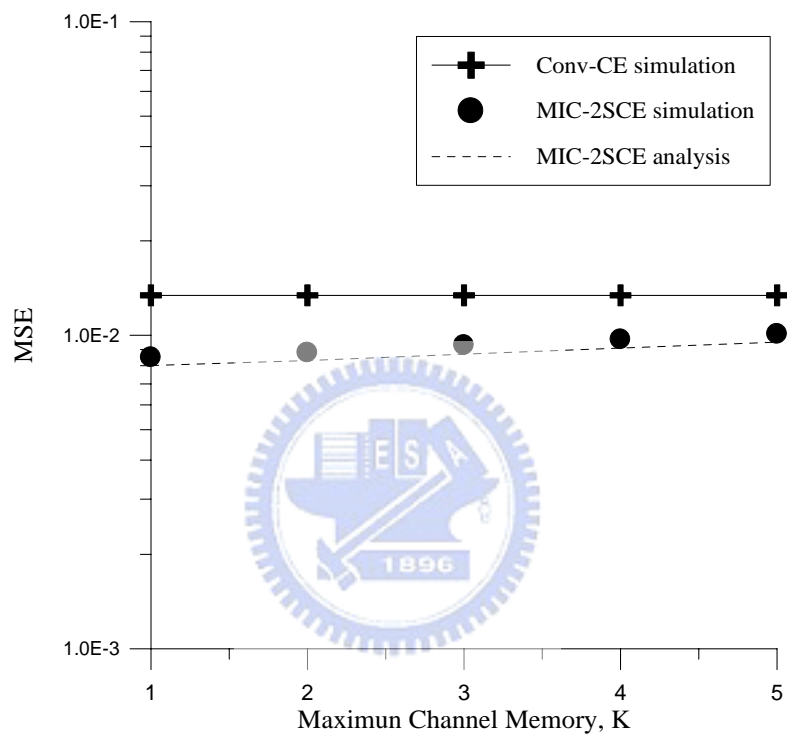


Fig. 3.4: MSE versus different maximum channel memory K in an equal-gain two-path channel at an SNR of 10 dB.

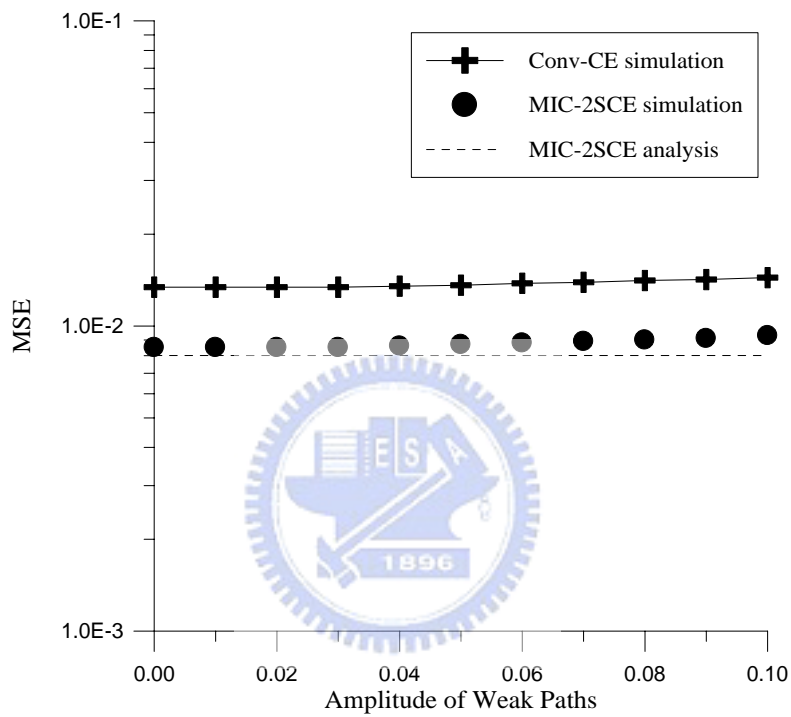


Fig. 3.5: MSE versus amplitude of the weaker paths in a multipath channel, this channel has two strong paths of equal power followed by two weaker paths also of equal power at an SNR of 10 dB.

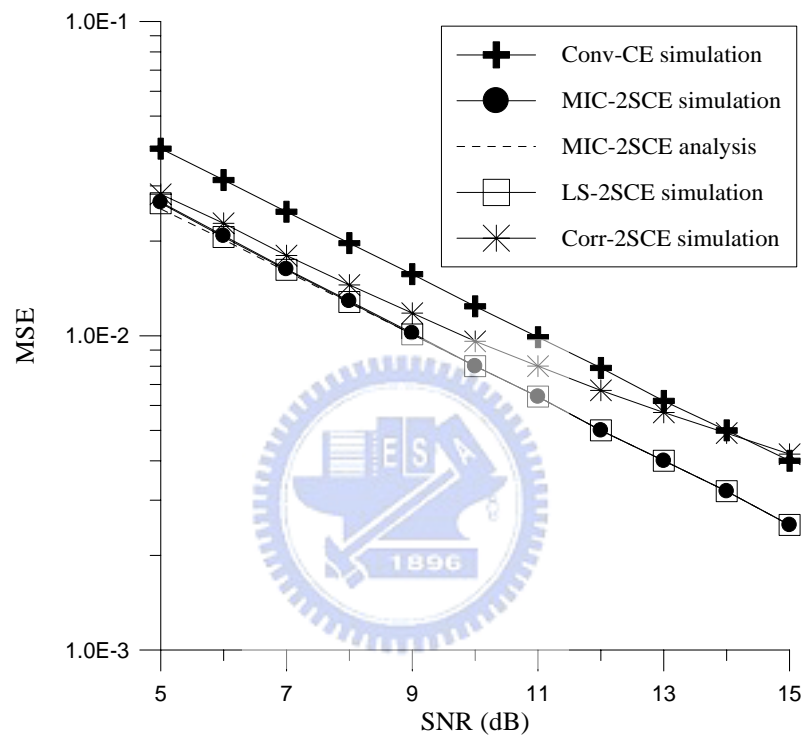


Fig. 3.6: MSE versus SNR in an equal-gain two-path fixed channel.

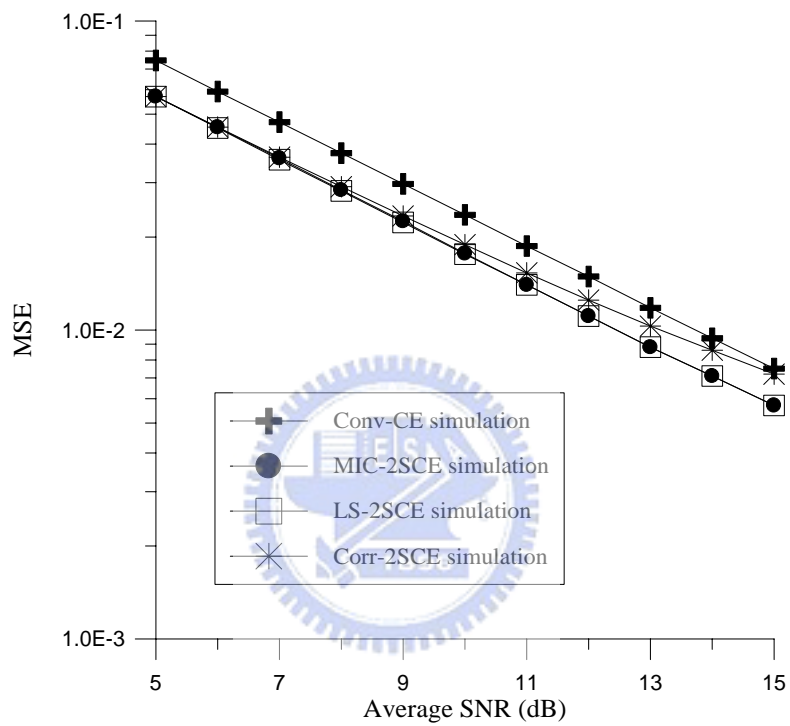


Fig. 3.7: MSE versus average SNR in a two-path (with equal average power) Rayleigh fading channel at the vehicle speed of 60 km/h.

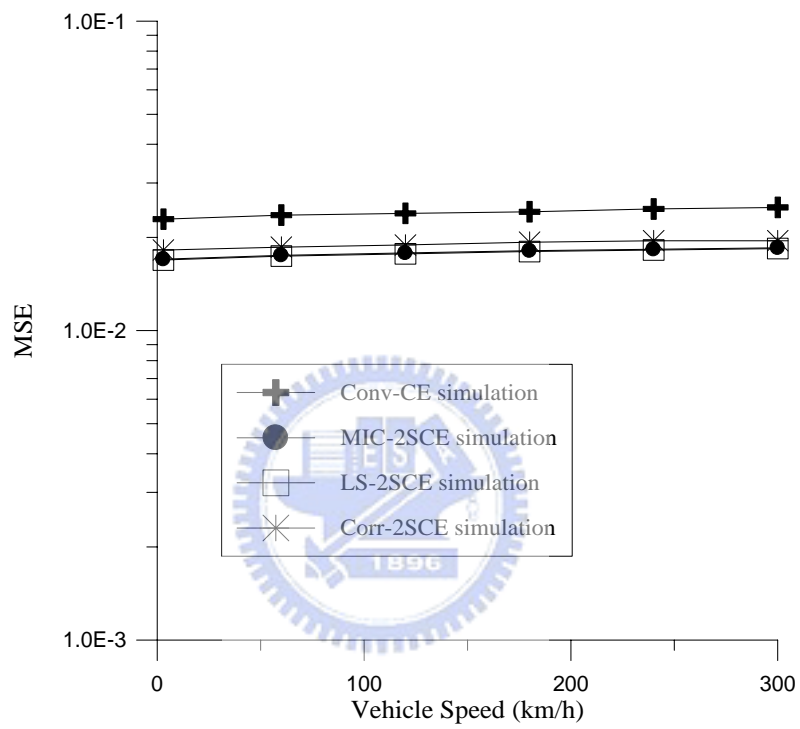


Fig. 3.8: MSE versus different vehicle speeds in a two-path fading channel at an average SNR of 10 dB.

# Chapter 4

## A Posterior Block Iterative Decision Feedback Detector

### 4.1 Introduction

The performance of a wireless communication system is significantly degraded by intersymbol interference (ISI) in a multipath fading channel. Since the multipath phenomenon in the radio channel provides multiple versions of original transmitted signal at a receiver, an effective way to improve the reliability of data reception is through the use of an implicit diversity combining technique which collects the signal energy from all the received signal paths [15]. In code division multiple access (CDMA) systems, implicit multipath diversity combining can be achieved by using a RAKE receiver [8], [13], [56]. In addition, some multi-user detection algorithms can be used to reconstruct the multiple access interference (MAI) contributed by other users, and then subtract the MAI from the received signals to further improve the detection capability of each individual user [20], [57], [58].

However, a RAKE receiver cannot be used in a time division multiple access (TDMA) system because there is no spreading code used in signal modulation and different multipath components cannot be resolved individually. In order to make the maximum use of the multipath components in TDMA systems, a novel posterior block iterative decision feedback detector is proposed in this paper. The whole detector is divided into a preliminary detector and a posterior detector. After the preliminary

detector, both the estimated channel impulse response (CIR) and preliminarily decided data are used jointly to calculate individual path interference and extract individual path signals. Maximal-ratio combining (MRC) technique is then used to combine these signals in a co-phased and weighted manner to get more reliable data. Furthermore, a soft decision is executed and its output is fed back to the detector to improve the system performance successively. Finally, a hard decision is made to get the final estimated data.

This chapter describes the system blocks, operation principles and evaluates the performance of the proposed method. In Section 4.2, the system model is described. In Section 4.3, the details of the proposed method including the function of each stage and the iterative manner are presented. Computer simulation results are presented in Section 4.4. Finally, discussion and conclusion are given in Section 4.5.

## 4.2 System Model

Here, we treat the transmitter filter, the channel, and the receiver filter together as an effective multipath channel for the transmitted data [9]. Consider a block-oriented data transmission system in such an effective multipath channel with a maximum delay spread of  $M$  samples, we have the equivalent baseband system block diagram of our proposed detector as shown in Fig. 4.1. Let the block length be  $L$ , then the length of the whole received signal sequence  $r[n]$  will be  $N = L + M - 1$ . For notational convenience, we represent most of the operations as a sequence operation, and hereafter we use zero padding to make all the sequences have a length of  $N$ . In this way, the linear convolution is equivalent to the circular convolution. Thus, we can use the circular convolution to represent linear convolution. Let a transmitted binary data sequence be denoted as  $d[n] = \{d_0, d_1, \dots, d_{L-1}, 0, \dots, 0_{N-1}\}$ , where  $d_i \in \{1, -1\}$ . The sequence  $r[n]$  can be expressed as below [59], [60]:

$$r[n] = d[n] \otimes h[n] + w[n] \quad (4.1)$$

where  $\otimes$  denotes a circular convolution operator, the complex CIR sequence is denoted as  $h[n] = \{h_0, h_1, \dots, h_{M-1}, 0, \dots, 0_{N-1}\}$ , and the  $N$ -point sequence  $w[n]$  denotes the additive white Gaussian noise (AWGN) with zero mean and variance  $\sigma_n^2$ .

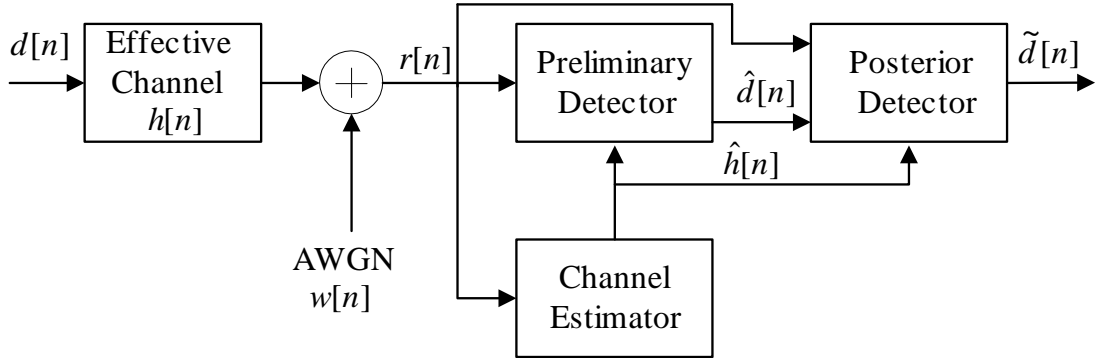


Fig. 4.1: An equivalent baseband system block diagram.

After the received signal sequence  $r[n]$  passes through a channel estimator and a preliminary data detector, the estimated CIR sequence  $\hat{h}[n]$  and the preliminarily decided data sequence  $\hat{d}[n]$  can be acquired. Afterwards, these two sequences together with the sequence  $r[n]$  are sent to the proposed detector.

### 4.3 The Proposed Detector

As shown in Fig. 4.2, the proposed posteriori detector is divided into four stages and each stage is described as follows:

- 1.) The first stage: Let the estimated CIR sequence be decomposed as

$$\hat{h}[n] = \hat{h}_0[n] + \hat{h}_1[n] + \dots + \hat{h}_{M-1}[n] \quad (4.2)$$

where  $\hat{h}_i[n]$  for  $i = 0, 1, \dots, M-1$  denote the individual path weight sequences which consist of a single value  $\hat{h}_i$  located at position  $i$  and zeros elsewhere. Accordingly, the circular convolution of  $\hat{h}_i[n]$  and  $\hat{d}[n]$  can be reduced to delay and multiplication operations. That is, each of the reconstructed individual path data sequence  $p_i[n]$  associated with path  $i$  can be written as

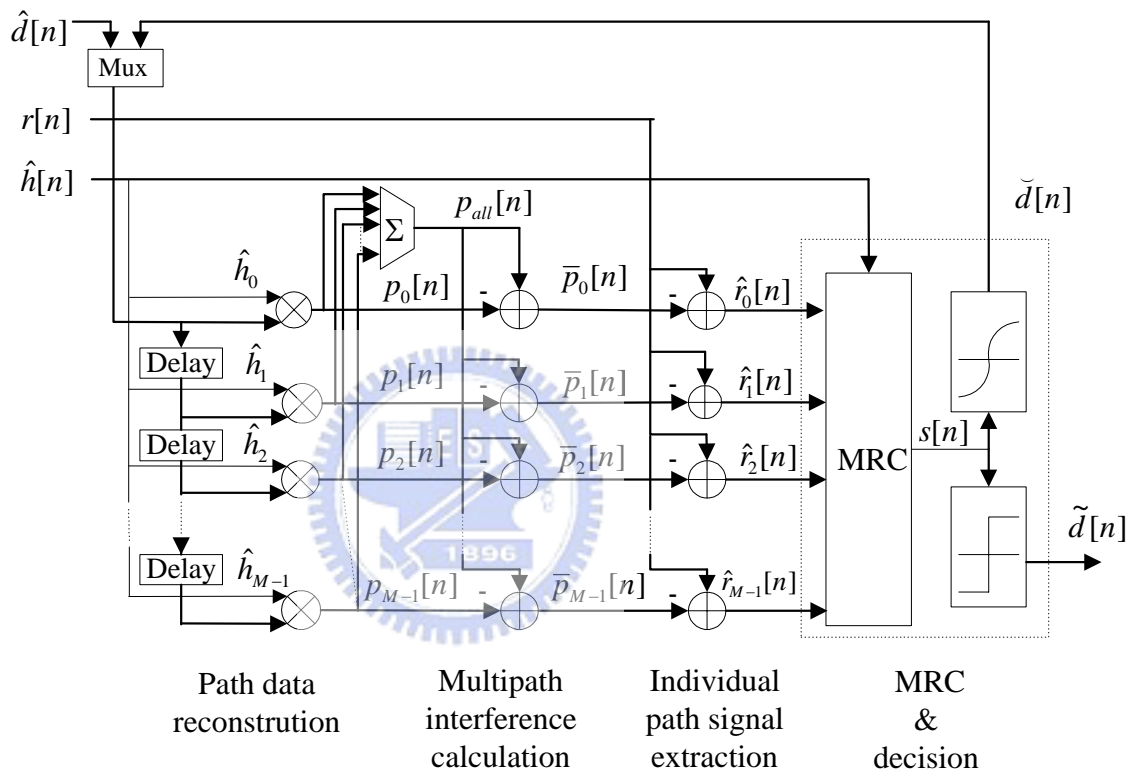


Fig. 4.2: Structure of the proposed posterior detector.

$$p_i[n] = \hat{d}[n] \otimes \hat{h}_i[n] = \hat{h}_i \hat{d}[\{(n-i)\}_N] \quad (4.3)$$

for  $i = 0, 1, \dots, M-1$ , where  $\{(n-i)\}_N$  denotes  $i$  points circular shift to the right of an  $N$ -point sequence. Then, an overall data sequence  $p_{\text{all}}[n]$  can be reconstructed by adding all the sequence  $p_i[n]$  together

$$p_{\text{all}}[n] = \sum_{i=0}^{M-1} p_i[n] = \hat{d}[n] \otimes \hat{h}[n] \quad (4.4)$$

2.) The second stage: The individual path interference sequences  $\bar{p}_i[n]$  for  $i = 0, 1, \dots, M-1$  can be calculated by subtracting sequence  $p_i[n]$  from the sequence  $p_{\text{all}}[n]$  as follows:

$$\bar{p}_i[n] = p_{\text{all}}[n] - p_i[n] \quad (4.5)$$

3.) The third stage: The individual path signal sequences  $\hat{r}_i[n]$  for  $i = 0, 1, \dots, M-1$  can be obtained by subtracting sequence  $\bar{p}_i[n]$  from the sequence  $r[n]$ , i.e.,

$$\begin{aligned} \hat{r}_i[n] &= r[n] - \bar{p}_i[n] \\ &= d[n] \otimes h[n] + w[n] - \hat{d}[n] \otimes \hat{h}[n] + \hat{d}[n] \otimes \hat{h}_i[n] \end{aligned} \quad (4.6)$$

4.) The fourth stage: The MRC operation can be represented as

$$s[n] = \sum_{i=0}^{M-1} \hat{h}_i^* \hat{r}_i[\{(n+i)\}_N] \quad (4.7)$$

where  $s[n]$  denotes the combined signal sequence and  $\{(n+i)\}_N$  denotes  $i$  points circular shift to the left of an  $N$ -point sequence. In an ideal situation, the estimated sequences  $\hat{d}[n] = d[n]$  and  $\hat{h}[n] = h[n]$ , then (4.6) will be reduced to  $\hat{r}_i[n] = d[n] \otimes h_i[n] + w[n]$ . Substitute it into (4.7) and after some algebraic operations, we get

$$s[n] = d[n] \sum_{i=0}^{M-1} |h_i|^2 + \sum_{i=0}^{M-1} h_i^* w[((n+i))_N] = d[n] + \sum_{i=0}^{M-1} h_i^* w[((n+i))_N] \quad (4.8)$$

where the power of CIR has been normalized to one, that is  $\sum_{i=0}^{M-1} |h_i|^2 = 1$ . Since all the circular noise components in (4.8) are independent at any sample instant, the total noise power will still be  $\sigma_n^2$ . In other words, the theoretic BPSK performance (the matched filter bound) can be achieved.

In practice, the preliminarily decided data sequence  $\hat{d}[n]$  is not ideal and a soft decision is used to reduce the effect of error propagation. The combined signal sequence  $s[n]$  is truncated to length L and sent to the soft decision block. Assume that the noise plus interference at the MRC output is a zero mean Gaussian random variable. At the  $k$  th sampling instant, a minimum mean square error criterion based soft decision function [61], [62] is used here to estimate the soft data information  $\check{d}_k$ , i.e.,

$$\check{d}_k = \tanh \left( s_k \frac{\sum_{i=0}^{M-1} |\hat{h}_i|^2}{s_k^2 - \sum_{i=0}^{M-1} |\hat{h}_i|^2} \right) \quad (4.9)$$

where the variance of noise plus interference is estimated by  $\left| s_k^2 - \sum_{i=0}^{M-1} |\hat{h}_i|^2 \right|$ . The soft decision output sequence  $\check{d}[n]$  is then fed back to the proposed detector for the next iteration. Finally, a hard decision is made to get the final estimated data sequence  $\tilde{d}[n]$ .

## 4.4 Simulation Results

To evaluate the performance of the proposed detector, a series of computer simulations were carried out under different channel conditions. Without loss of generality, the GSM packet format was employed for convenience [20]. Accordingly, the block data length L was set to 148 and the maximum CIR length M was set to 6. The carrier frequency was set to 900 MHz and the BPSK modulation method was simulated at a data rate of 270.833 kbit/sec. The power of CIR was normalized to one.

Two-path channels [63] were assumed and modeled in such a way that the first path was at the first sample and the second path was at the second sample. Two different kinds of detectors were employed as preliminary detectors: a zero forcing (ZF) equalizer [16] and an minimum mean square error based decision feedback equalizer (MMSE\_DFE) (jointly optimizing the tap weights of both the feedforward and feedback filters with a priori knowledge of the CIR) [64], [65]. A soft decision was used at the output of each preliminary detector. The simulation results corresponding to the ZF detector were plotted as solid lines and those corresponding to the MMSE\_DFE detector were plotted as dash lines.

In the first set of simulations, the performance of the proposed detector in a two-path fixed channel with the second path smaller than the first path by 3 dB was examined. The SNR per bit was varied from 6 to 11 dB and the ideally estimated CIR was assumed. The corresponding results are shown in Fig. 4.3. It is clearly observed that the bit error rate (BER) of the ZF preliminary detector plus posterior detector (ZF+PD) outperforms the ZF detector, and the BER performance of the MMSE\_DFE preliminary detector plus posterior (MMSE\_DFE+PD) outperforms the MMSE\_DFE detector. Also, the BER performances of both the ZF+PD and the MMSE\_DFE+PD detectors become better and better as iteration time increases. This is because more reliable data can be detected with each iteration and it can be used to reconstruct more accurate multipath interference. Accordingly, a more precise individual path signal can be extracted and a better MRC gain can be acquired. It is worth pointing out that because the channel condition is not too severe for a linear equalizer to handle, the BER performance of the ZF+PD detector performs well and it outperforms the MMSE\_DFE detector as iteration time increases.

In the second set of simulations, the performance of the proposed detector in an equal-gain two-path fixed channel was examined. The SNR per bit was varied from 6 to 11 dB and the ideally estimated CIR was assumed also. The corresponding results are shown in Fig. 4.4. It is clearly observed that the BER performance of the ZF+PD detector outperforms the ZF detector, and the BER performance of the MMSE\_DFE+PD detector outperforms the MMSE\_DFE detector. The BER performances of the two iterative detectors also become better and better as iteration time increases. Since the transfer function of the channel in this case has spectral nulls

and it results in a large noise enhancement at the output of the ZF detector, the BER performance suffers from a high error floor. Though the BER performance of the ZF+PD detector becomes better as iteration time increases; it is still inferior to the MMSE\_DFE detector which generates much less noise enhancement as compared with the ZF detector.

In the third set of simulations, the performance of the proposed detector in a two-path (with equal average power) Rayleigh fading channel was evaluated. The average SNR per bit was varied from 10 to 20 dB and the estimated CIR was obtained by means of the correlation method [26]. Note that the complex gains of the two fading paths were generated independently by using Jake's fading channel model [51], at a vehicle speed of 60 km/h. The corresponding results are shown in Fig. 4.5. It is clearly observed that the BER performance of the ZF+PD detector outperforms the ZF detector, and the BER performance of the MMSE\_DFE+PD detector outperforms the MMSE\_DFE detector. The BER performances of the two iterative detectors again become better and better as iteration time increases. In addition, the fading phenomenon reduces the probability of spectral nulls of the effective channel. Therefore, the noise enhancement is reduced at the output of the ZF detector and the BER performance of the ZF+PD detector approaches that of the MMSE\_DFE detector as iteration time increases.

## 4.5 Discussion and Conclusion

In this chapter, a novel posterior detector for digital wireless communication systems is proposed. The structure of the preliminary detector together with the posterior detector is similar to that of a decision feedback equalizer (DFE) [14]–[16] which is composed of a feedforward filter and a feedback filter. There are three major differences between our detector and a DFE as following:

- 1.) The inputs to this proposed detector are the estimated CIR sequence, the preliminarily decided data and the received signal sequence. That is, a preliminary detector and a channel estimator are needed in the proposed detector. As a comparison, the input to a DFE is the received signal only.
- 2.) The proposed detector can be used to extract each individual path signal by

subtracting the reconstructed multipath interference from the received signal, and then make a maximal ratio combining (MRC) to achieve the multipath diversity gain. In contrast, the feedback filter of a DFE exploits the previously detected symbols to suppress the ISI in the present symbol for data detection and it does not provide the multipath diversity gain.

- 3.) The proposed detector can be operated in an iterative way [66]. Since a more reliable decided data can be used to reconstruct a more accurate multipath interference. Accordingly, a more precise individual path signal can be extracted and a better MRC gain can be acquired. Therefore, a soft decision is executed and its output is fed back to our detector to improve the system performance successively. In contrast, a conventional DFE cannot be operated in an iterative manner.

In addition, the structure of the proposed detector has an advantage over a DFE in that it can be easily modified to a tap-selectable structure [64]–[66] in which a path selection unit and variable delay elements are used. In other words, the computation complexity can be greatly reduced as compared with a DFE when the multipath channel has a sparse impulse response and a long delay spread [67]–[69].

Computer simulations were done to evaluate the performance of the proposed detector with two different kinds of preliminary detectors. Simulation results indicate that the proposed detector can achieve implicit diversity gains in both fixed and fading multipath channels and its BER performance is clearly improved with successive iterations. It is noteworthy that the preliminary detector used by the proposed scheme can be of any kind of detectors. Moreover, the proposed detector structure can be easily modified and used in a CDMA RAKE receiver to further improve its detection capability.

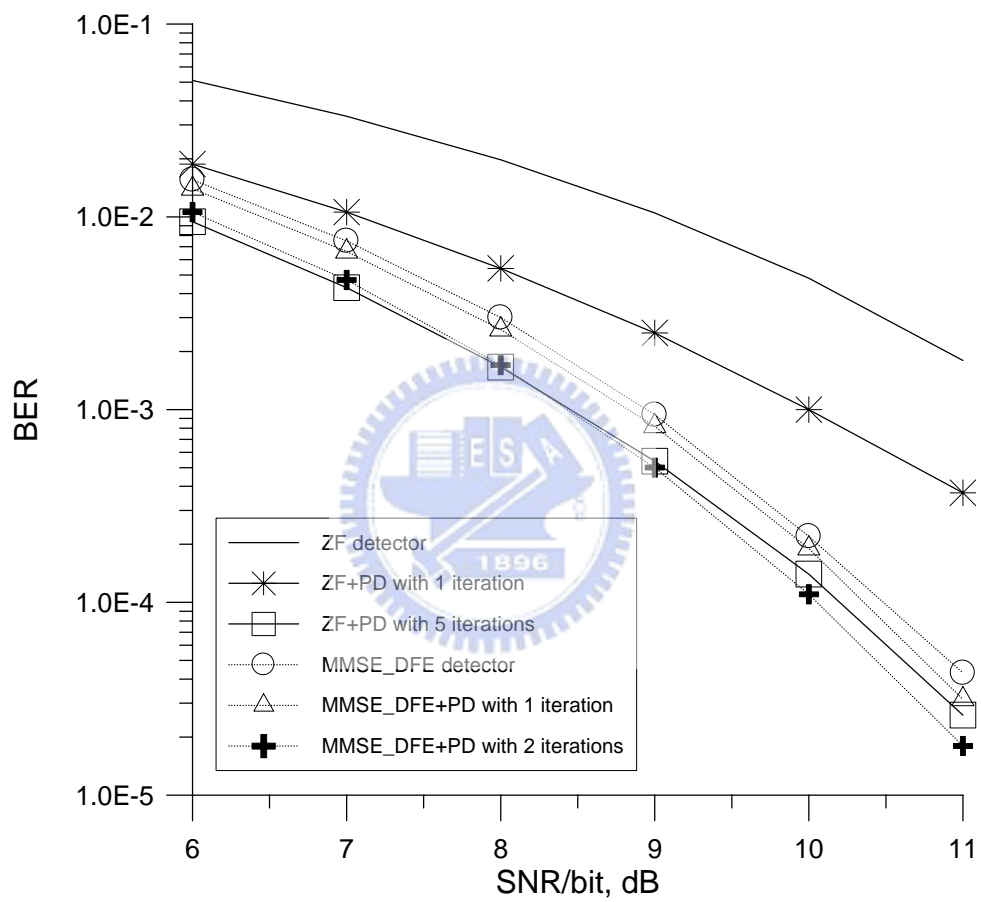


Fig. 4.3: BER performance in a two-path fixed channel with the second path smaller than the first path by 3 dB.

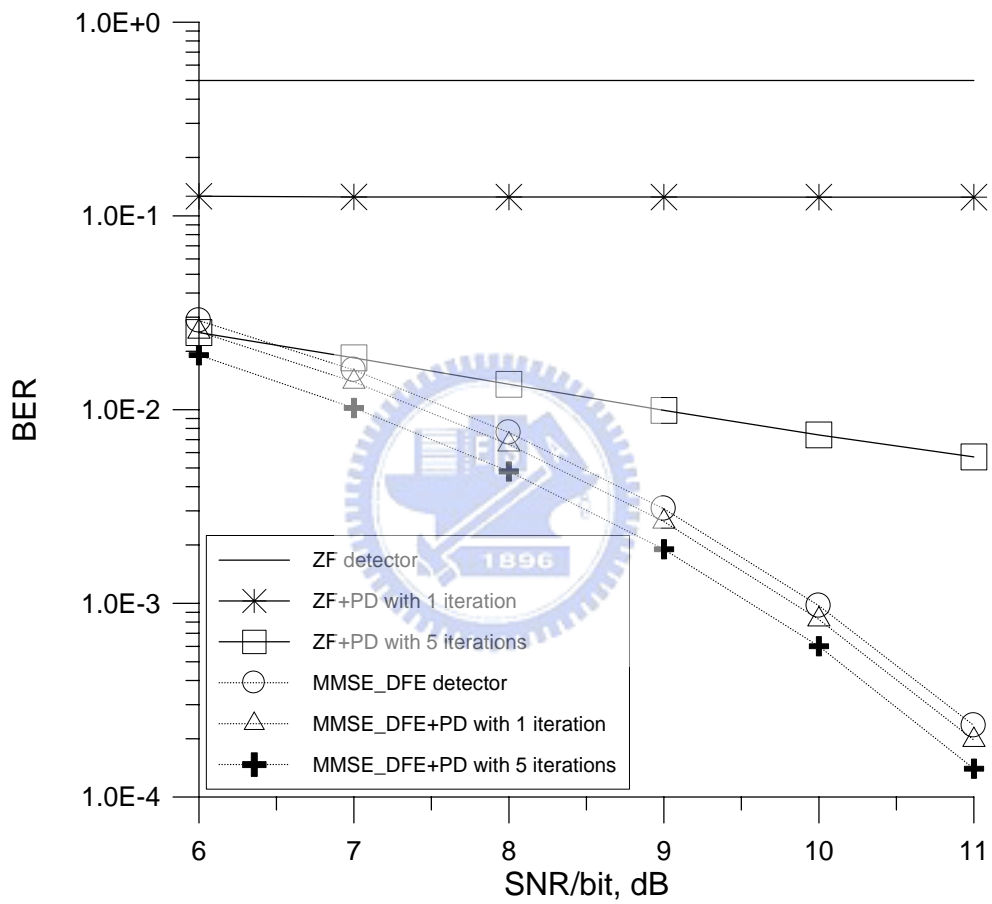


Fig. 4.4: BER performance in an equal-gain two-path fixed channel.

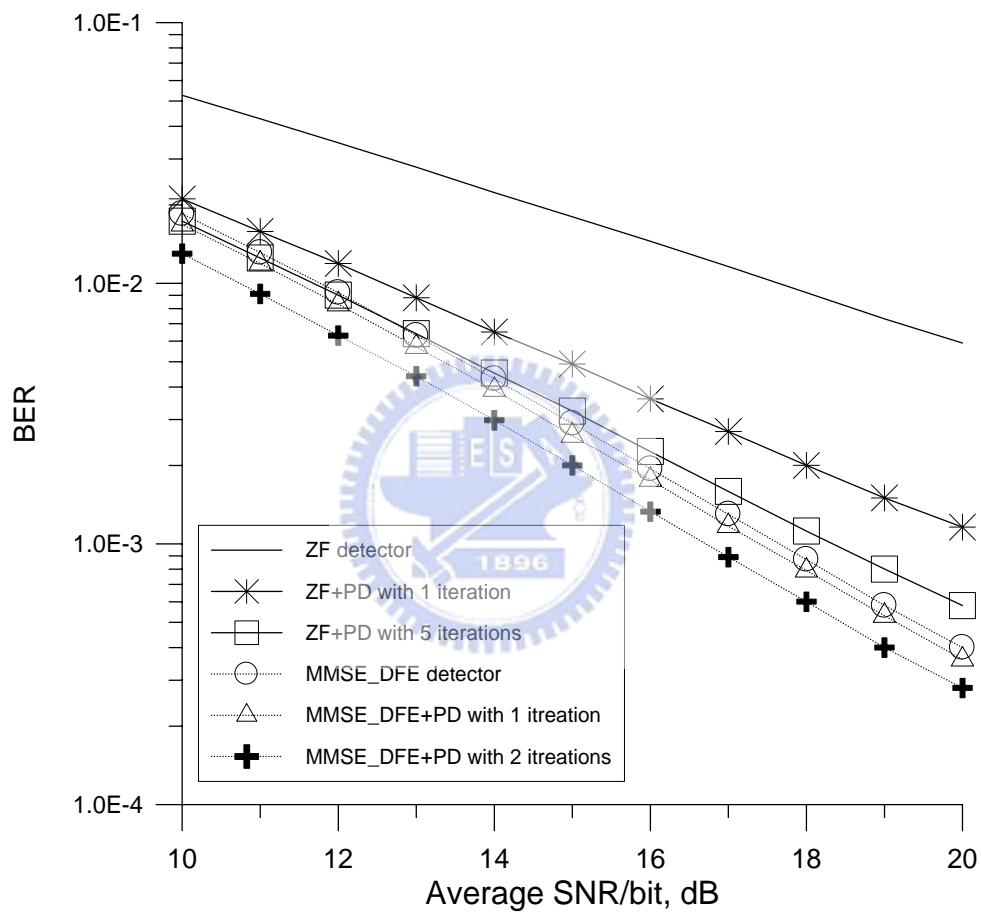


Fig. 4.5: BER performance in a two-path Rayleigh fading channel at a vehicle speed of 60 km/h.

# Chapter 5

## Conclusion and Future Research

### 5.1 Conclusion

Two channel estimation methods and one posterior detector for digital wireless communications are presented in this dissertation. All these methods can be used to enhance the equalization ability of the receiver in digital wireless communications and thereby improve the BER performance of the transmission system.

In Chapter 2, a novel LS-2SCE method is proposed in order to fully utilize the uncorrupted data in the guard interval for channel estimation. The proposed method was designed as a two-stage procedure. In the first stage, the LS algorithm was used to compute the initial CIR estimation based on the normal training sequence, and then the maximum channel memory could be estimated. In the second stage, the estimated maximum channel memory was used to extract the uncorrupted data in the guard interval. Finally, the extended normal training sequence was sent to the LS algorithm again to estimate a fine-tuned CIR. Both a theoretical analysis and computer simulations were carried out to confirm that the proposed LS-2SCE method outperforms the Conv-CE method.

In Chapter 3, a novel MIC-2SCE method is proposed to avoid relatively high computation complexity in processing the LS algorithm in the second stage of the LS-2SCE method. Jointly using the knowledge of maximum channel memory and effective paths which have been estimated in the first stage, the individual path interference could be reconstructed, and then the individual path signal could be

extracted in the region corresponding to the extended normal training sequence. Therefore, the correlation method could be used to estimate a fine-tuned CIR in the second stage. Both theoretical analysis and computer simulations confirm that the proposed method outperforms the Conv-CE method. Furthermore, from our simulation results and discussion on computation complexity, it is clear that the MIC-2SCE method has approximately equal MSE performance as that of the LS-2SCE method but it has a lower computation complexity.

In Chapter 4, a novel posterior detector for digital wireless communication systems is proposed. The whole detector is divided into a preliminary detector and a posterior detector. After the preliminary detector, the preliminarily decided data and estimated CIR could be acquired. Jointly using these corresponding results, the individual path interference could be calculated and the individual path signals could be extracted. Then, maximal-ratio combining (MRC) technique was used to combine these signals to get more reliable data. Furthermore, a soft decision was executed and its output was sent back to the posterior detector to improve the system performance successively. Computer simulation results indicate that the proposed detector can achieve implicit diversity gains in both fixed and fading multipath channels and its BER performance is clearly improved with successive iterations. It is noteworthy that the preliminary detector used by the proposed scheme can be of any kind of detectors.

## 5.2 Future Research

The channel estimation and posterior detection techniques presented in this dissertation are general and can be used for most TDMA systems. There are several related topics which could be addressed:

- 1.) The two stage channel estimation methods can be easily modified and applied to OFDM systems. In OFDM systems, a guard interval which is a cyclic extension of an OFDM pilot symbol is included in the serial data stream in order to keep this pilot symbol away from ISI during its transmission [40], [41]. The structure of the whole OFDM symbol (including the guard interval) is similar to that of the training sequence as depicted in Fig. 2.1. Therefore, the two stage channel estimation methods can be employed to make a more accurate channel estimation.

- 2.) The purpose of the first stage of the LS-2SCE method is to find the maximum channel memory  $K$ . Therefore, it is not necessary to execute the Conv\_CE method to obtain an initial estimated CIR in the first stage if other methods [73] can be used to obtain the maximum channel memory  $K$ .
- 3.) The two stage channel estimation methods and the posterior detector can be used jointly in parallel to improve the system performance. As two-stage channel estimation method makes more accurate channel estimation, and this may help the preliminary detector to make more correct data detection. Furthermore, it helps the posterior detector to make more precise data reconstruction, multipath interference calculation and signal extraction, and the detection ability of the posterior detector will also be enhanced.
- 4.) The architecture of the posterior detector can be modified to be a tap-selectable structure [67] in which a path selection unit and variable delay elements are used. The computation complexity of the modified architecture only increases linearly with the number of the effective paths. Therefore, it may be a good structure with relative low computation complexity when the multipath channel has a sparse impulse response and a long delay spread [70].
- 5.) The channel decoder and deinterleaver can be included in the posterior detector to further improve the system performance. From that point of view, the combined structure is similar to the structure of a turbo equalizer. Also, when a tap-selectable structure of the posterior detector is used, the computation complexity of the combined structure can be greatly lower than a conventional turbo equalizer when the multipath channel has a sparse impulse response and a long delay spread.

# Appendix

## Derivation of the Mean Square Error Associated with the $k$ th Path

Taking the expectation of the difference between the estimated path gain  $\tilde{h}_k$  and true path gain  $h_k$  according to equation (3.11), the mean square error (MSE) associated with the  $k$ th path can be written as

$$\begin{aligned}
 \text{MSE}_k &= E \left\{ \left| \tilde{\mathbf{s}}_k^H [\tilde{\mathbf{n}} - \tilde{\mathbf{S}}\mathbf{D}_k (\mathbf{S}^H \mathbf{S})^{-1} \mathbf{S}^H \mathbf{n}] / \tilde{N} \right|^2 \right\} \\
 &= E \left\{ \tilde{\mathbf{s}}_k^H [\tilde{\mathbf{n}} - \tilde{\mathbf{S}}\mathbf{D}_k (\mathbf{S}^H \mathbf{S})^{-1} \mathbf{S}^H \mathbf{n}] [\tilde{\mathbf{n}} - \tilde{\mathbf{S}}\mathbf{D}_k (\mathbf{S}^H \mathbf{S})^{-1} \mathbf{S}^H \mathbf{n}]^H \tilde{\mathbf{s}}_k \right\} / \tilde{N}^2 \\
 &= 1 / \tilde{N}^2 \times \left\{ \tilde{\mathbf{s}}_k^H E \{ \tilde{\mathbf{n}} \tilde{\mathbf{n}}^H \} \tilde{\mathbf{s}}_k - \tilde{\mathbf{s}}_k^H E \{ \tilde{\mathbf{n}} \mathbf{n}^H \} \mathbf{S} (\mathbf{S}^H \mathbf{S})^{-1} \mathbf{D}_k \tilde{\mathbf{S}}^H \tilde{\mathbf{s}}_k - \tilde{\mathbf{s}}_k^H \tilde{\mathbf{S}} \mathbf{D}_k (\mathbf{S}^H \mathbf{S})^{-1} \mathbf{S}^H E \{ \mathbf{n} \tilde{\mathbf{n}}^H \} \tilde{\mathbf{s}}_k + \right. \\
 &\quad \left. \tilde{\mathbf{s}}_k^H \tilde{\mathbf{S}} \mathbf{D}_k (\mathbf{S}^H \mathbf{S})^{-1} \mathbf{S}^H E \{ \mathbf{n} \mathbf{n}^H \} \mathbf{S} (\mathbf{S}^H \mathbf{S})^{-1} \mathbf{D}_k \tilde{\mathbf{S}}^H \tilde{\mathbf{s}}_k \right\} \\
 &= \sigma_n^2 / \tilde{N}^2 \times \\
 &\quad \left\{ \tilde{N} - \tilde{\mathbf{s}}_k^H \begin{bmatrix} \mathbf{O} \\ \mathbf{I} \end{bmatrix} \mathbf{S} (\mathbf{S}^H \mathbf{S})^{-1} \mathbf{D}_k \tilde{\mathbf{S}}^H \tilde{\mathbf{s}}_k - \tilde{\mathbf{s}}_k^H \tilde{\mathbf{S}} \mathbf{D}_k (\mathbf{S}^H \mathbf{S})^{-1} \mathbf{S}^H [\mathbf{O} \quad \mathbf{I}] \tilde{\mathbf{s}}_k + \tilde{\mathbf{s}}_k^H \tilde{\mathbf{S}} \mathbf{D}_k (\mathbf{S}^H \mathbf{S})^{-1} \mathbf{D}_k \mathbf{S}^H \tilde{\mathbf{s}} \right\}
 \end{aligned} \tag{A.1}$$

where  $E\{\cdot\}$  denotes the expectation operator,  $|\cdot|$  denotes the absolute operator, and the expectation  $E\{\tilde{\mathbf{n}} \tilde{\mathbf{n}}^H\} = \sigma_n^2 [\mathbf{O}_{N \times (\tilde{N}-N)} \quad \mathbf{I}_{N \times N}]$ . Let us further define an  $L \times 1$  vector  $\mathbf{f} = [1_0 \quad 1_1 \quad \cdots \quad 1_{L-1}]^T$  to rewrite

$$[\mathbf{O} \quad \mathbf{I}] \tilde{\mathbf{s}}_k = \mathbf{S}(\mathbf{I} - \mathbf{D}_k) \mathbf{f} \tag{A.2}$$

Substituting (A.2) into (A.1), the MSE associated with the  $k$ th path becomes

$$\begin{aligned}
\text{MSE}_k &= \sigma_n^2 / \tilde{N}^2 \times \left\{ \tilde{N} - \mathbf{f}^H (\mathbf{I} - \mathbf{D}_k) \mathbf{S}^H \mathbf{S} (\mathbf{S}^H \mathbf{S})^{-1} \mathbf{D}_k \tilde{\mathbf{S}}^H \tilde{\mathbf{s}}_k - \tilde{\mathbf{s}}_k^H \tilde{\mathbf{S}} \mathbf{D}_k (\mathbf{S}^H \mathbf{S})^{-1} \mathbf{S}^H \mathbf{S} (\mathbf{I} - \mathbf{D}_k) \mathbf{f} + \right. \\
&\quad \left. \tilde{\mathbf{s}}_k^H \tilde{\mathbf{S}} \mathbf{D}_k (\mathbf{S}^H \mathbf{S})^{-1} \mathbf{D}_k \mathbf{S}^H \tilde{\mathbf{s}}_k \right\} \\
&= \sigma_n^2 / \tilde{N}^2 \times \left\{ \tilde{N} - \mathbf{f}^H (\mathbf{I} - \mathbf{D}_k) \mathbf{D}_k \tilde{\mathbf{S}}^H \tilde{\mathbf{s}}_k - \tilde{\mathbf{s}}_k^H \tilde{\mathbf{S}} \mathbf{D}_k (\mathbf{I} - \mathbf{D}_k) \mathbf{f} + \tilde{\mathbf{s}}_k^H \tilde{\mathbf{S}} \mathbf{D}_k (\mathbf{S}^H \mathbf{S})^{-1} \mathbf{D}_k \mathbf{S}^H \tilde{\mathbf{s}}_k \right\} \\
&= \sigma_n^2 / \tilde{N}^2 \times \left\{ \tilde{N} + \tilde{\mathbf{s}}_k^H \tilde{\mathbf{S}} \mathbf{D}_k (\mathbf{S}^H \mathbf{S})^{-1} \mathbf{D}_k \tilde{\mathbf{S}}^H \tilde{\mathbf{s}}_k \right\} \tag{A.3}
\end{aligned}$$



# Bibliography

- [1] W. C. Y. Lee, *Essentials of Wireless Communications*, McGraw-Hill, Inc. 2001.
- [2] S. Weinstein and A.D. Gelman, "Network multimedia: issues and perspectives," *IEEE Commun. Mag.*, pp. 138–143, June 2003.
- [3] Y. Kim, B. J. Jeong, J. Chung, C-S Hwang, J. S. Ryu and Y. K. Kim, "Beyond 3G: vision, requirements, and enabling technologies," *IEEE Commun. Mag.*, pp. 120–124, Mar. 2003.
- [4] K. Ahmavaara, H. Haverinen and R. Pichna, "Interworking architecture between 3GPP and WLAN systems," *IEEE Commun. Mag.*, pp. 74–81, Nov. 2003.
- [5] S. Haykin, *Communication Systems*, John Wiley & Sons, 2001.
- [6] R.E. Ziemer and W. H. Tranter, *Principles of Communications*, John Wiley & Sons, Inc., 2002.
- [7] R. Sklar, *Digital Communications – Fundamentals and Applications*, NJ: Prentice Hall, 1988.
- [8] T. S. Rappaport, *Wireless Communications, Principles & Practice*, NJ: Prentice-Hall, 1996.
- [9] J. W. Mark and W. Zhuang, *Wireless Communications and Networking*, NJ: Prentice-Hall, 2003.
- [10] B. Sklar, "Rayleigh fading channels in mobile digital communication systems, part I: characterization," *IEEE Commun. Mag.*, pp. 90–100, July 1997.
- [11] B. Sklar, "Rayleigh fading channels in mobile digital communications systems,

- part II: mitigation,” *IEEE Commun. Mag.*, pp. 102–109, July 1997.
- [12] T. Kumagai and K. Kobayashi, “Postdetection maximal ratio combining diversity receiver with scalar phase signals”, *IEEE 6th International Conference on*, San Diego, Oct. 1997, pp. 391–395.
- [13] Y. Akaiwa, *Introduction to Digital Mobile Communication*, John Wiley & Sons, 1997.
- [14] S. Haykin and M. Moher, *Modern Wireless Communications*, Prentice Hall, 2004.
- [15] K. Pahlavan and A. H. Levesque, *Wireless Information Networks*, John Wiley & Sons, Inc., 1995.
- [16] J. G. Proakis, *Digital Communications*, 4th ed. NY: McGraw-Hill, 2001.
- [17] R. Koetter, A. C. Singer and M. Tüchler, “Turbo equalization,” *IEEE signal Processing Mag.*, pp. 67–80, Jun. 2004.
- [18] M. Tüchler, R. Koetter and A.C. Singer, “Turbo equalization: principles and new results,” *IEEE Trans. Commun.*, vol. 50, no. 5, pp. 754–767, Dec. 2002.
- [19] C. Laot, A. Glavieux and J. Labat, “Turbo equalization: adaptive equalization and channel decoding jointly optimized,” *IEEE Trans. Commun.*, vol. 19, no. 9, pp. 1744–1752, Sep. 2001.
- [20] S. Moshavi, “Multi-user detection for DS-CDMA communications,” *IEEE Commun. Mag.*, vol. 34, pp. 124–136, Oct. 1996.
- [21] A. Duel-Hallen, J. Holtzman and Z. Zvonar, “Multiuser detection for CDMA Systems,” *IEEE Pers. Commun.*, vol. 2, pp. 46–58, Apr. 1995.
- [22] A. Papoulis, *Probability, Random Variables, and Stochastic Processes*. McGraw-Hill, Inc. 1991.
- [23] G. D’Arla and V. Zingarelli, “Results on fast-Kalman and Viterbi adaptive equalizers for mobile radio with CEPT/GSM system characteristics,” in *Proc. Globecom 88, Hollywood, USA*, Dec. 1988, pp. 815–819.
- [24] G. D’Arla, R. Piermarini and V. Zingarelli, “Fast adaptive equalizers for

- narrow-band TDMA mobile radio,” *IEEE Trans. Veh. Technol.*, vol. 40, no. 2, pp. 392–404, May 1991.
- [25] G. D’Aria, F. Muratore, and V. Palestini, “Simulation and performance of the Pan-European land mobile radio system,” *IEEE Trans. Veh. Technol.*, vol. 41, no. 3, pp. 177–189, May 1992.
- [26] E. Yakhnich, “Channel estimation for EGPRS modems,” in *Proc. VTC’01*, Rhodes, Greece, May 2001, pp. 419 – 422.
- [27] M. Pukkila, Channel Estimation Modeling, Nokia research center, Fall 2000.
- [28] C. Luschi, M. Sandell, P. Strauch, J. J. Wu, C. Ilas, P. W. Ong, R. Baeriswyl, F. Battaglia, S. Karageorgis, and R. H. Yan, “Advanced signal-processing algorithms for energy-efficient wireless communications,” *Proc. IEEE*, vol. 88, no. 10, pp. 1633–1650, Oct. 2000.
- [29] N. Nefedov and M. Pukkila, “Iterative channel estimation for GPRS,” in *Proc. PIMRC’00*, vol. 2, London, UK, Sep. 2000, pp. 999–1003.
- [30] P. Strauch, C. Luschi, and A. M. Kuzminskiy, “Iterative channel estimation for EGPRS,” in *Proc. VTC’00*, Boston, USA, Sep. 2000, pp. 2271–2277.
- [31] M. Sandell, C. Luschi, P. Strauch, and R. Yan, “Iterative channel estimation using soft decision feedback,” in *Proc. Globecom 98*, Sydney, Australia, Nov. 1998, pp. 3728–3733.
- [32] M. Skoglund, J. Giese, and S. Parkvall, “Code design for combined channel estimation and error protection,” *IEEE Trans. Inform. Theory*, vol. 48, no. 5, pp. 1162–1171, May 2002.
- [33] K. D. Kammeyer, V. Kuhn, and T. Petermann, “Blind and nonblind turbo estimation for fast fading GSM channels,” *IEEE J. Select. Areas Commun.*, vol. 19, no. 9, pp. 1718–1728, Sep. 2001.
- [34] T. S. Rappaport, S. Y. Seidel, and R. Singh, “900-MHz multipath propagation measurements for U.S. digital cellular radiotelephone,” *IEEE Trans. Veh. Technol.*, vol. 39, no. 1, pp. 132–139, May 1990.

- [35] R. D'Avella, L. Moreno, and M. Sant'Agostino, "An adaptive MLSE receiver for TDMA digital mobile radio," *IEEE J. Select. Areas Commun.*, vol. 7, no. 1, pp. 122–129, Jan. 1989.
- [36] 3GPP, "Physical layer aspects of UTRA high speed downlink packet access", TR25.848, V4.0.0, Mar. 2001.
- [37] K Higuchi., A. Fujiwara and M. Sawahashi, "Multipath interference canceller for high-speed packet transmission with adaptive modulation and coding scheme in W-CDMA forward link", in *IEEE VTC 2001 Spring*, May, 2001, pp 2297–2301.
- [38] K Higuchi., A. Fujiwara and M. Sawahashi, "Multipath interference canceller for high-speed packet transmission with adaptive modulation and coding scheme in W-CDMA forward link", *IEEE J. Select. Areas Commun.*, vol. 20, no. 1, pp. 419–432, Feb. 2002.
- [39] C. W. Therrien, *Discrete Random Signals and Statistical Signal Processing*, NJ: Prentice-Hall, 1992.
- [40] IEEE, "Part 11: Wireless LAN Medium and Physical layer (PHY) specifications: High-speed Physical Layer in the 5 GHz Band," IEEE Std. 802.11a-1999, Sep. 1999.
- [41] ETSI, "Digital Video Broadcasting (DVB); Frame structure, channel coding and modulation for digital terrestrial television," ETSI EN 300 744, V1.4.1, Jan. 2001.
- [42] E. G. Larsson and J. Li, "Preamble design for multiple-antenna OFDM-based WLANs with null subcarriers," *IEEE Signal Processing Lett.*, vol. 8, no. 11, pp. 285–288, Nov. 2001.
- [43] X. Wang and K. J. Ray Liu, "Adaptive channel estimation using cyclic prefix in multicarrier modulation system," *IEEE Commun. Lett.*, vol. 3, no. 10, pp. 291–293, Oct. 1999.
- [44] W. Chen and U. Mitra, "Training sequence optimization: comparisons and an alternative criterion," *IEEE Trans. Commun.*, vol. 48, no. 12, pp. 1987–1991,

Dec. 2000.

- [45] S.M. Kay, *Fundamentals of Statistical Signal Processing: Estimation Theory*, Prentice-Hall, 1998.
- [46] S. N. Crozier, D. D. Falconer, and S. A. Mahmoud, “Least sum of squared errors (LSSE) channel estimation,” *IEE Proceeding-f*, vol. 138, no. 4, pp. 371–378, Aug. 1991.
- [47] C. C. Chen and C. C. Huang, “Fast feedforward channel sounding RAKE receiver,” *Electron. Lett.*, vol. 36, no. 20, pp. 1731–1733, Sep. 2000.
- [48] A. J. Viterbi, *CDMA: Principles of Spread Spectrum Communication*, Addison Wesley, 1995.
- [49] B. Kolman and D. R. Hill, *Elementary Linear Algebra*, NJ: Prentice Hall, 2000.
- [50] S. Haykin, *Adaptive Filter Theory*, 3rd ed., NJ: Prentice-Hall, 1996.
- [51] W. C. Jakes, *Microwave Mobile Communications*, Wiley, New York, 1974.
- [52] P. Fan and M. Darnell, *Sequence Design for Communication Applications*, Research Studies Press Ltd., 1996.
- [53] E. H. Dinan and B. Jabbari, “Spreading codes for direct sequence CDMA and wideband CDMA cellular networks”, *IEEE Commun. Mag.*, pp. 48–54, Sep. 1998.
- [54] W. J. Lin, T. T. Lin, and C. C. Huang, “A novel two-stage channel estimation method for wireless communications,” *IEICE Trans. Commun.*, vol.E87-B, no. 6, pp. 1479–1486, June 2004.
- [55] G. H. Golub and C. F. Van Loan, *Matrix Computations*, The Johns Hopkins University Press, Baltimore and London, 1989.
- [56] Z. Zvonar, “Combined multiuser detection and diversity reception for wireless CDMA system,” *IEEE Trans. Veh. Technol.*, vol. 45, pp. 205–211, Feb. 1996.
- [57] S. Verdu, *Multiuser Detection*. Cambridge, UK: Cambridge University Press, 1998.

- [58] C. W. Huang and K. A. Wen, "A low-complexity 3-stage parallel interference cancellation receiver (LCPIC) for DS-CDMA cellular systems," in *Proc. VTC'01, Atlantic City, NJ*, Oct. 2001, pp. 853 – 857.
- [59] J. G. Proakis and D. G. Manolakis, *Digital Signal Processing*. NJ: Prentice-Hall, 1996.
- [60] A.V. Oppenheim and R. W. Schaffer, *Discrete-Time Signal Processing*, NJ: Prentice-Hall, 1989.
- [61] S. L. Ariyavisitakul, and Y. Li, "Joint coding and decision feedback equalization for broadband wireless channels," *IEEE J. Select. Areas Commun.*, 1998, pp. 1670–1678.
- [62] S. Y. Wang, "On design and simulation of FFT-based RAKE receiver architectures for wideband CDMA systems," Ph.D. dissertation, National Chiao Tung University, Hsinchu, Taiwan, June 2001.
- [63] S. Y. Wang and C. C. Huang, "On the architecture and performance of an FFT based spread downlink RAKE receiver," *IEEE Trans. Veh. Technol.*, vol. 50, pp. 234–243, Jan. 2001.
- [64] N.W. K. Lo, D. D. Falconer and A. U. H. Sheikh, "Adaptive equalization for co-channel interference in a multipath fading environment," *IEEE Trans. Commun.*, vol. 43, no. 2/3/4, pp. 1441–1453, Feb./Mar./Apr. 1995.
- [65] C. Tidestav, M. Sternad and A. Ahlen, "Reuse within a cell -- interference rejection or multiuser detection," *IEEE Trans. Commun.*, vol. 47, no.10, pp. 1511–1522, Oct. 1999.
- [66] Albert M. Chan, and Gregory W. Wornell, "A class of block-iterative equalizers for intersymbol interference channels: Fixed channel results", *IEEE Trans. Commun.*, vol. 49, no. 11, pp. 1966-1976, Nov. 2001.
- [67] S. Ariyavisitakul, N. R. Sollenberger and L. J. Greenstein, "Tap-selectable decision feedback equalization," *IEEE Trans. Commun.*, vol. 45, no. 12, pp. 1497–1997, Dec. 1997.
- [68] S. Ariyavisitakul, and L. J. Greenstein, "Reduced-complexity equalization

- techniques for broadband wireless channels,” *IEEE J. Select. Areas Commun.*, vol. 15, no.1, pp. 5–15, Jan. 1997.
- [69] S. Ariyavisitakul, and L. J. Greenstein, “Reduced-complexity equalization techniques for broadband wireless channels,” in *IEEE ICC’97*, Montreal, P. Q. , Canada, June 1997, pp. 1521–1526.
- [70] S. F. Cotter and B. D. Rao, “Sparse channel estimation via matching pursuit with application to equalization,” *IEEE Trans. Commun.*, vol. 50, no. 3, pp. 374–377, Mar. 2002.
- [71] R. Cusani and J. Mattila, “Equalization of digital radio channels with large multipath delay for cellular land mobile applications,” *IEEE Trans. Commun.*, vol. 47, no. 3, pp. 348–351, Mar. 1999.
- [72] I. J. Fevrier, S. B. Gelfand and M. P. Fitz, “Reduced complexity decision feedback equalization for multipath channels with large delay spreads,” *IEEE Trans. Commun.*, vol. 47, no. 6, pp. 927–937, June 1999.
- [73] C. R. Sheu and C. C. Huang, “A novel guard interval based ISI-free sampling region detection method for OFDM systems,” in *IEEE VTC 2004*, Los Angeles, Sept. 2004.